THE CONSTRUCTION OF A FLAT FLAME BURNER AND MEASUREMENT OF ADIABATIC FLAME SPEED

by

Jack A. Neuberger

A Thesis Submitted to the Faculty of the

DEPARTMENT OF AEROSPACE AND MECHANICAL ENGINEERING

In Partial Fulfillment of the Requirements
For the Degree of

MASTER OF SCIENCE

In the Graduate College

THE UNIVERSITY OF ARIZONA

1 9 6 5

STATEMENT BY AUTHOR

This thesis has been submitted in partial fulfillment of requirements for an advanced degree at The University of Arizona and is deposited in the University Library to be made available to borrowers under rules of the Library.

Brief quotations from this thesis are allowable without special permission, provided that accurate acknowledgment of source is made. Requests for permission for extended quotation from or reproduction of this manuscript in whole or in part may be granted by the head of the major department or the Dean of the Graduate College when in his judgment the proposed use of the material is in the interests of scholarship. In all other instances, however, permission must be obtained from the author.

SIGNED: Jack A. Newberger

APPROVAL BY THESIS DIRECTOR

This thesis has been approved on the date shown below:

R.E. Petersen
R. E. PETERSEN
Associate Professor of Aerospace and Mechanical Engineering

APRIL 13, 1965
Date

ACKNOWLEDGMENTS

The author wishes to express his appreciation to Dr. Russell E. Petersen for the many helpful suggestions, unlimited patience, and guidance which permitted the accomplishment of this thesis project.

In addition, deep gratitude is extended to my wife Carmen, and my children Catherine, Cynthia, Carmen Lea, Christine, and Mary Jo for their sacrifices during the course of my study which is completed with the writing of this document.

TABLE OF CONTENTS

	Page
LIST OF ILLUSTRATIONS	v
ABSTRACT	viii
CHAPTER	
I. INTRODUCTION	1
A. History	1
B. General Theory	8
II. DESCRIPTION OF APPARATUS	17
A. Construction of Burner	17
B. Arrangement of Equipment	21
C. Method of Measurement	25
III. EXPERIMENTAL PROCEDURE	32
A. Operation of Burner	32
B. Test Results	35
C. Discussion of Test Results	43
IV. CONCLUSIONS AND RECOMMENDATIONS	52
SYMBOLS	56
REFERENCES	58

LIST OF ILLUSTRATIONS

Figure		Page
1.1	Powling's Flat Flame Burner	3
1.2	Hoelscher's Flat Flame Burner	7
1.3	Different Positions of the Flame Front in Its Movement Towards the Porous Disc	9
1.4	Temperature Distribution for the Different Positions of the Flame Front in Figure 1.3 .	9
1.5	Extrapolation of Flame Speed to Adiabatic Conditions	11
1.6	Range of Application of Particle Track Technique	15
2.1	Two inch Diameter Flat Flame Burner with Concentric Water Jackets	18
2.2	Schematic of Equipment for Burner System . .	22
2.3	Burner Mounted in Combustion Tunnel	24
2.4	Cooling Water System Control Panel	24
2.5	Potentiometer, Thermocouple Junction, and Cooling Baths	26
2.6	Air/Fuel System Control Panel	26
3.1	Characteristic Flat Flame; V_u = 0.607 ft/sec, A/F = 15.6, Q = 2420 Btu/lbm	33
3.2	Semi-diffusion Flame on Top of Flat Flame Burner; V_u = 0.484 ft/sec, A/F = 8.79, Q = 484 Btu/lbm	33
3.3	Initial Cell Formation; V_u = 0.485 ft/sec, A/F = 9.10, Q = 581 Btu/lbm	33

LIST OF ILLUSTRATIONS--Continued

Page

3.4 Isolation of Cells by Non-luminous Ridges; V_u = 0.485 ft/sec, A/F = 9.15, Q = 607 Btu/lbm 33

3.5 Number of Cells Increases; V_u = 0.487 ft/sec, A/F = 10.20, Q = 753 Btu/lbm 38

3.6 Individual Cells Join at Their Tips; V_u = 0.488 ft/sec, A/F = 10.31, Q = 780 Btu/lbm 38

3.7 Flattening Out of Flame Front; V_u = 0.490 ft/sec, A/F = 10.76, Q = 907 Btu/lbm 38

3.8 Flat Flame Front; V_u = 0.495 ft/sec, A/F = 11.26, Q = 1017 Btu/lbm 38

3.9 Initial Buckling and Frayed Edges; V_u = 0.503 ft/sec, A/F = 25.56, Q = 434 Btu/lbm 39

3.10 Rigid Distortion Near Blow-off; V_u = 0.504 ft/sec, A/F = 28.47, Q = 289 Btu/lbm 39

3.11 Blow-off; V_u = 0.506 ft/sec, A/F = 29.13, Q = 222 Btu/lbm 39

3.12 Formation of High Dark Ridges Between Cells; V_u = 1.495 ft/sec, A/F = 10.05, Q = 193 Btu/lbm 39

3.13 Non-luminous Ridges Start to Decay; V_u = 1.497 ft/sec, A/F = 13.91, Q = 289 Btu/lbm 42

3.14 Continuous Corrugated Flame Front; V_u = 1.498 ft/sec, A/F = 14.09, Q = 308 Btu/lbm 42

3.15 Formation of Concentric Ring or Wave; V_u = 0.130 ft/sec, A/F = 8.10, Q = 1350 Btu/lbm 42

LIST OF ILLUSTRATIONS--Continued

Page

3.16 Tight, Non-concentric Packing at High Flow Speeds; V_u = 1.330 ft/sec, A/F = 13.80, Q = 309 Btu/lbm 42

3.17 Heat Carried Away Versus Air/Fuel Ratio for Different Mixture Speeds 44

3.18 Values of Mixture Speed for the Curves of Figure 3.17 at an Air/Fuel Ratio of 14.95 . . 46

3.19 Flame Speed as a Function of Q for Different A/F Ratios on the Lean Side of A/F = 14.95 . 49

3.20 Flame Speed as a Function of Q for Different A/F Ratios on the Rich Side of A/F = 14.95 . 50

ABSTRACT

This thesis project involves the design and construction of an apparatus which has the capability of producing a flat flame and the experimental determination of adiabatic flame speed. In the case of a flat flame burner a one-dimensional flame is closely approximated by the formation of a thin disc-like sheet of flame downstream from the burner. The burner is constructed so that a mixture of propane and air emanates from a porous plug which is cooled by various water jackets. Appropriate adjustment of mixture ratios and mixture velocities yields a balance between the propagation of the flame front and the rate at which the unburned gases enter the flame front. This allows the resultant flat flame to assume a position of equilibrium a short distance from the burner port. The flame may be stabilized by controlling heat extraction over a wide range of mixture ratios and mixture flow speeds; adiabatic flame speeds are then obtained by a method of extrapolating to zero heat extraction.

By the injection of magnesium oxide dust particles into the unburned mixture stream it is possible to obtain photographic measurements of stream velocities which may be used to obtain local flame speeds.

The experimental results obtained are in agreement with those of other sources.

CHAPTER I

INTRODUCTION

A. History

In the past, a number of methods have been developed to measure the speed of laminar flame propagation of pre-mixed gaseous air/fuel mixtures. Some of these techniques involve data obtained from the bunsen burner, glass-tube combustion, soap-bubble combustion, and the spherical bomb. None of these methods are entirely satisfactory, and all but one technique involve measurements made on a curved flame front. In the case of the tube method, friction due to the movement of the flame through the tube is a factor which influences the flame propagation. Also, the heat transfer to the walls of the tube would have an effect on the flame speed in an obscure fashion.

The one method which has been found to be more satisfactory than any of the others is the flat flame burner technique. A flat or plane flame has the distinct advantage of eliminating the problem of measurements along a curved surface. Furthermore, not only does the flame burn above a flat surface in the configuration of a disc, but also the reaction zone of the flame is free from all surface contacts thereby eliminating any additional assumptions which would compromise determination of accurate data.

In 1948, Dr. Powling (21)* studied the laminar propagation of slow burning flames across a flat or planar reaction zone. His burner was based on two principal requirements for obtaining a flat flame. First, the reacting gases should be made to issue from the burner with as uniform a velocity distribution as is possible with freedom from viscous effects at the burner tube walls. Second, the flow patterns of the reaction zone should be undisturbed by the hot products of combustion.

In Figure 1.1 is shown Dr. Powling's burner. A pre-mixed explosive gas mixture enters the base of a water-cooled copper burner and the flow is distributed uniformly across the entire tube diameter by a diffuser which consists of a short section of glass beads followed by a series of fine gauzes. The gases are then conducted to a position short of the burner port through a vertically laminated matrix made from a roll of alternately plain and corrugated metal tape which fulfills the requirement of streamlining the flow pattern. The distance of the matrix from the burner port is so adjusted that the velocity distribution becomes fairly uniform except for slight viscous effects at the very edges of the flame.

---

*Numbers in parentheses refer to cited references.

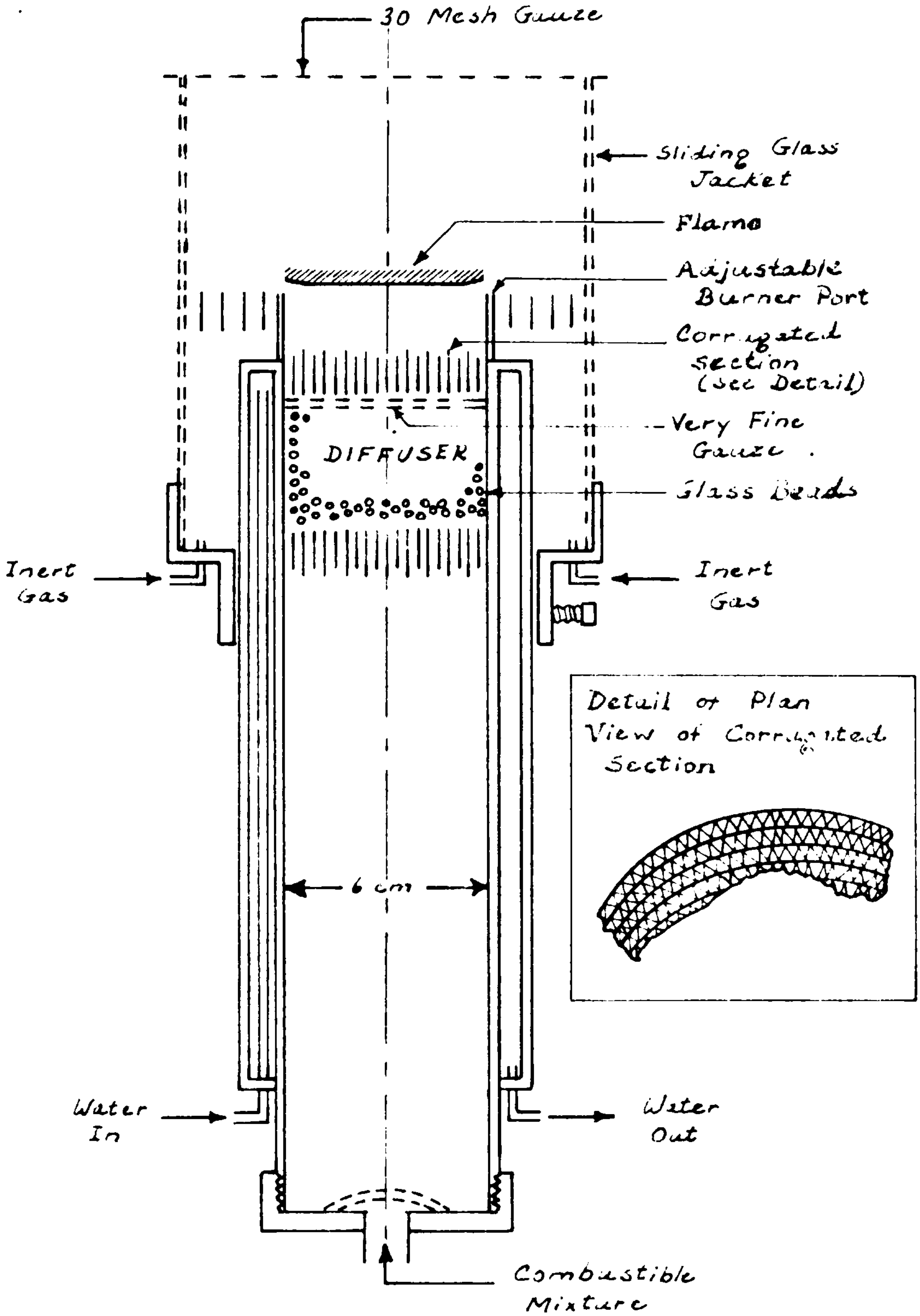

Figure 1.1 Powling's Flat Flame Burner

Nonuniformity in the edges is corrected just above the burner port by injecting a flow of inert gas between the sliding glass jacket and the adjustable burner port. With this technique a relatively flat flame was obtained above the burner port free from contact with any surface provided that a suitable resistance, usually in the form of a 30 mesh gauze, was placed in the path of the rapidly rising combustion products. Without this resistance, there was a tendency of the cooler surrounding air to displace the less dense products of combustion resulting in disturbances being propagated into the unburnt gases to such an extent that the production of a stable flat flame was impossible. Powling surmised that this may be the very reason why low velocity flames have not been previously stabilized on a burner.

By controlling the mixture flow it was possible to match the approach speed of the unburned mixture with that of the flame propagation speed, thereby obtaining a stable flame. Unfortunately, Powling's burner had limited application in that it was possible to produce a flat flame only over a flame speed range of from 5 to 10 centimeters per second.

In 1951, Egerton and Thabet (2) studied laminar flame propagation experimentally with the aid of a modified version of Powling's flat flame burner. These studies included the measurement of burning rates of slow flames ranging from 4 to 12 centimeters per second and the determination of the limits of combustion. The inert gas stream which was utilized by Powling was eliminated by Egerton and Thabet. The reason for this was that Dr. Thabet found no evidence substantiating the necessity for using such a stream of inert gas.

In 1954, Botha and Spalding (1) developed a burner which produced a flat flame over a wide range of mixture ratios with flame speeds ranging from 4 to 38 centimeters per second. This extension in the range of flame speeds which could be measured was a distinct improvement. The distinguishing feature of the Botha and Spalding burner is a water-cooled disc of porous metal through which the combustible mixture is forced. In the case of the Powling burner, the problem was one of regulating the mixture speed so that it exactly equals the flame speed. Unfortunately, this balancing became impossible when the flame speed exceeded about 12 centimeters per second. In the Botha and Spalding burner, no difficulty is encountered in balancing the mixture speed against the flame speed; the mixture speed is merely made slower than the free space flame speed so that the flame which forms upon ignition travels upstream toward the porous disc. As the flame approaches the disc it begins to transfer heat to the disc which, being very effectively cooled, does not rise in temperature by more than a few degrees. The heat transfer to the disc necessarily reduces the temperature of the burned gas and consequently results in a reduction in flame speed. The flame then rapidly and automatically takes up a position of equilibrium a short distance above the disc where the flame loses just enough heat to reduce its propagation speed to match the mixture speed and thereby establish a flat flame.

Other burners have subsequently been developed but it was not until 1957 that Hoelscher (12) created a significant departure from the basic designs of Powling or Botha and Spalding. In the case of the Hoelscher burner, the speed of the inlet mixture exceeds the flame speed at the throat of the burner. Beyond the throat, the stream tubes expand so that a point of balance is reached where the increased cross section reduces the speed of the mixture to that of the flame. The adjustable plate above the burner, as shown in Figure 1.2, serves to suppress the tendency of the flame to form a conical shape by providing a flat reference surface. The Hoelscher burner has the distinct advantage of simplicity of construction with the added benefit of a greater latitude of control over the location of the flat flame with respect to the burner lip. By adjusting the plate height and holding all other variables constant, the flame can be made to move relative to the burner lip. However, this burner is limited to air/fuel ratios on the lean side of stoichiometric and flame speeds of from 4.4 to 8.5 centimeters per second.

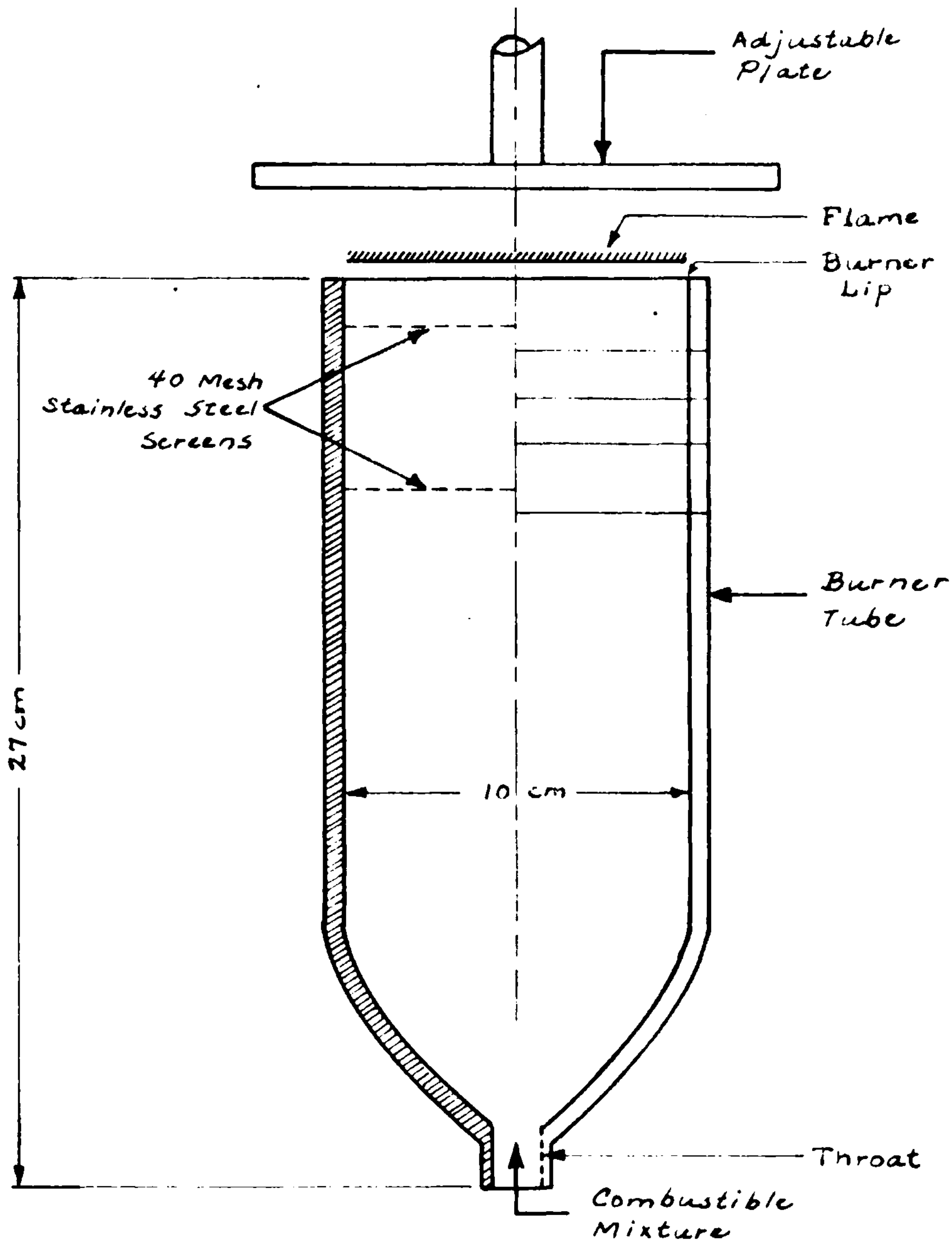

Figure 1.2 Hoelscher's Flat Flame Burner

The approach described in this thesis is basically a modification of that developed by Botha and Spalding.

B. General Theory

The basic theory behind the design of the burner used in this project is as follows: A water-cooled disc of fine sintered porous metal allows the passage of a combustible mixture. If the porosity is fine and even, the emerging stream of gas from the disc may be taken as uniform. When the gas is ignited downstream, a flame is formed which travels upstream if the flame speed exceeds the mixture speed and conversely, travels downstream if the mixture speed is greater than the flame speed. Figure 1.3 illustrates the successive positions of the flame front after ignition as it approaches the porous plate from the downstream direction and Figure 1.4 then shows the corresponding temperature in the porous disc and the burned region (1). When the flame nears the disc, an increasing quantity of heat is transferred to the disc which, being effectively cooled, does not rise in temperature by more than a few degrees. However, as is shown in Figure 1.4, the temperature of the burned gases is reduced, resulting in a reduction of flame speed. This loss in heat results in the flame assuming a condition of equilibrium a short distance above the porous disc.

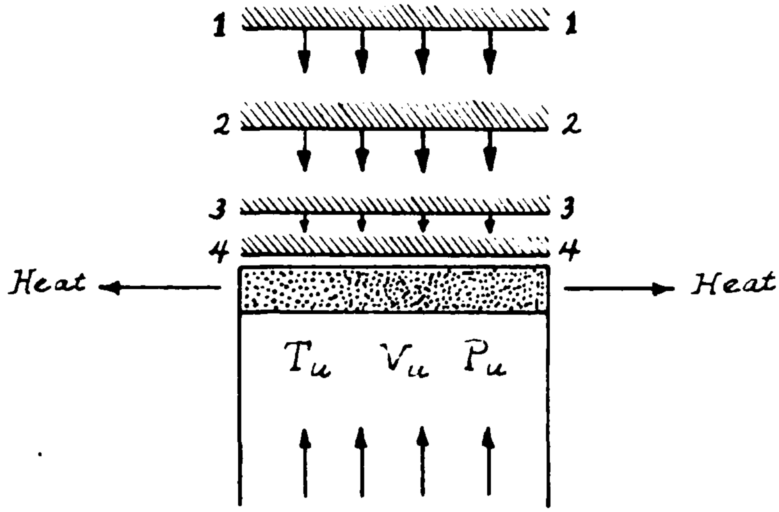

Figure 1.3 Different Positions of the Flame Front in Its Movement Towards the Porous Disc (Ref. 1)

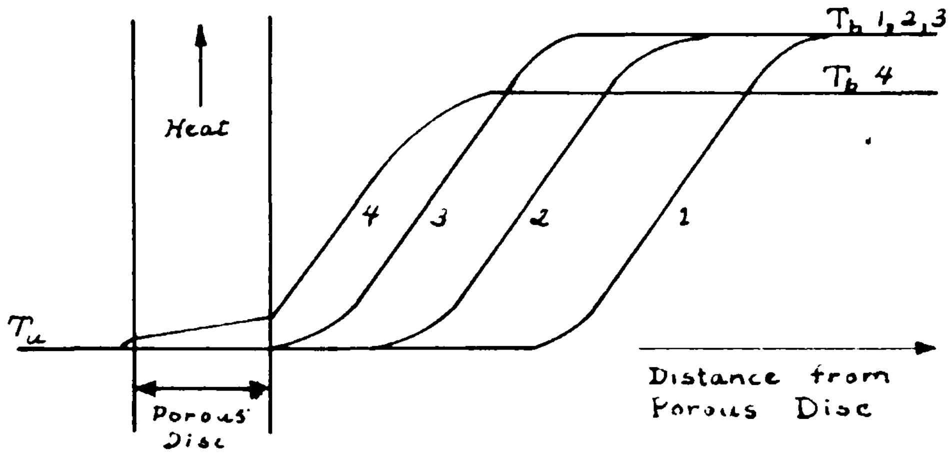

Figure 1.4 Temperature Distribution for the Different Positions of the Flame Front in Figure 1.3 (Ref. 1)

Obviously, the heat carried away by the cooling water through the disc must be measured, and the flame speed, uncorrected for the adiabatic condition, must also be determined. The flame speed is evaluated by dividing the volumetric flow rate of the propane-air mixture by the area of the plane flame front, which may be measured photographically. It is then possible to plot curves of flame speeds versus heat extracted for a given air/fuel ratio and to extrapolate the resulting curve to zero heat loss or adiabatic conditions. Figure 1.5 illustrates such a curve (1).

A characteristic of the porous-disc burner is that a large amount of heat is removed when the unburned mixture speed, V_u, is small; whereas when the mixture speed is increased to approach that of the laminar adiabatic flame speed, S_u, of the mixture, the heat transfer rate to the porous metal disc decreases. In fact, when V_u equals or exceeds S_u, the flame does not remain plane but distorts in a manner which will be discussed in detail in Chapter III. The greater the distortion of the flame, the greater the increase of V_u with accompanying heat losses to the porous disc. Obtaining a value of S_u has been done with considerable accuracy by Botha and Spalding by extrapolating the linear portion of the V_u versus Q plot (Fig. 1.5) in which the air/fuel ratio is held constant. The upper curved portion of the V_u versus Q plot is neglected

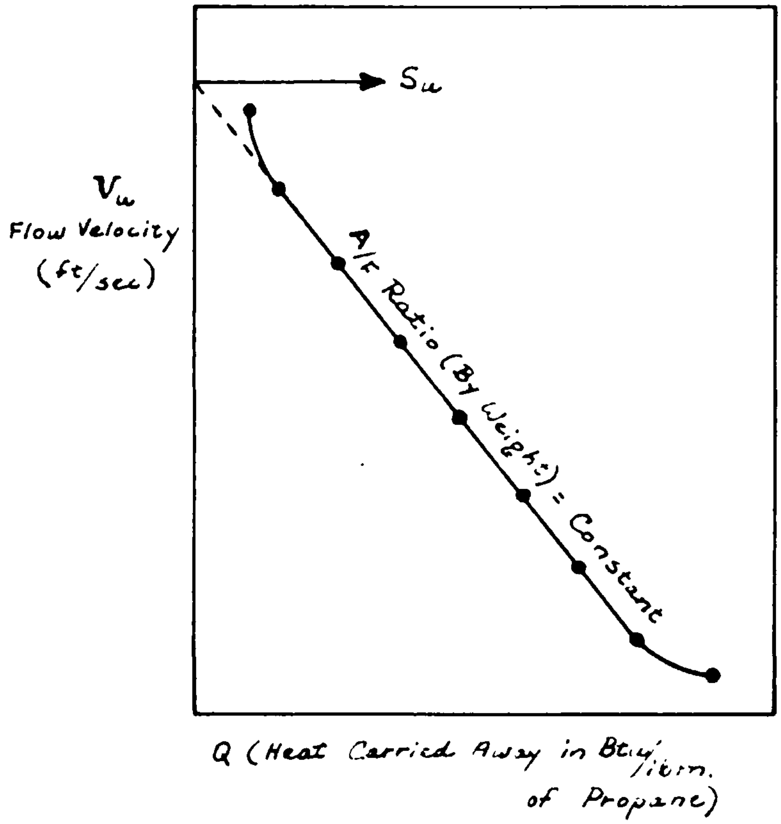

Figure 1.5 Extrapolation of Flame Speed to Adiabatic Conditions

in the extrapolation because of spurious local curvature effects.

It should be noted that this procedure may also be carried out for various air/fuel ratios and the laminar adiabatic flame speed may be evaluated for each air/fuel ratio.

In addition, flame speed observations may be obtained by injecting microscopic magnesium oxide dust particles into the mixture stream upstream of entering the burner and illuminating these with stroboscopic light. The geometry of the flat flame would appear to permit easy visualization of the paths of the particles (which should appear as dashes). Photographic recordings of these particle tracks would allow direct measurement of stream velocity, and such particle track data would provide a check of flame speeds obtained from dividing the volumetric flow rate by the flame area; once again the flame speed obtained would have to be corrected to an adiabatic condition in order to ascertain the laminar adiabatic flame speed.

This visualization of a flow system by injecting dust particles is a fairly standard technique in aerodynamic studies and has been applied to flames by a number of authors (2, 7-9, 13, 23-25). Measurement of velocity is possible using photography properly timed with illumination devices. The distance a particle travels is obtained from a series of dashes and the velocity is derived by dividing distance between successive dashes by the time between dashes.

The errors introduced by the particle track method can be classified under three headings: physical effects on the flame, chemical effects on the flame, and errors due to the particle failing to follow the gas stream.

Particle injection has the following physical effect on the flame. If particle type, size, and number are not carefully regulated, the flame might be extinguished by the absorption of heat due to the thermal capacity of the particles and by their radiation.

The chemical effects of particles on a flame are more difficult to establish. A particle could act as an accelerator or as an inhibitor and hence it could change the course of the reaction. Because of the short residence time in the flame front, the chemical effects can be made negligible by reducing the particle density.

With regard to the particle failing to follow the gas stream, the flame gases and tracer particles are strongly accelerated when passing through a flame front. This acceleration force must be balanced by aerodynamic drag caused by slippage of the particle relative to the carrier gas. The order of magnitude of this error may be estimated by equating the forces of acceleration with the particle drag. Extensive studies have been conducted by

Fristrom and Westenberg (7) regarding this question. It was deduced that there are two major types of errors: acceleration lag and thermomechanical effects.

Acceleration lag can be related to the mass and size of the particles and maximum drag occurs when particles are large compared with the mean free path.

Thermomechanical effect is a force which particles experience in a temperature gradient and results from the unbalance in molecular collisions on the hot and cold side of a particle. This effect falls off sharply when the particle becomes large compared with the mean free path. In practice, particles should be chosen to be large compared with the mean free path.

A compromise between acceleration lag and thermomechanical effect results in restricting the quantitative use of particle track studies in flames. Fristrom and Westenberg's results are expressed in Figure 1.6 which displays the range of applicability of particle track studies to flame front aerodynamics. Figure 1.6 applies if a precision of three per cent is acceptable. Where higher precision is required, it is advisable to investigate other methods. The region of applicability is determined as follows: Burning velocity in centimeters per second is plotted against particle radius in microns. The region for satisfactory particle track studies (error less than 3%) at 0.1 atmosphere is cross-hatched. To

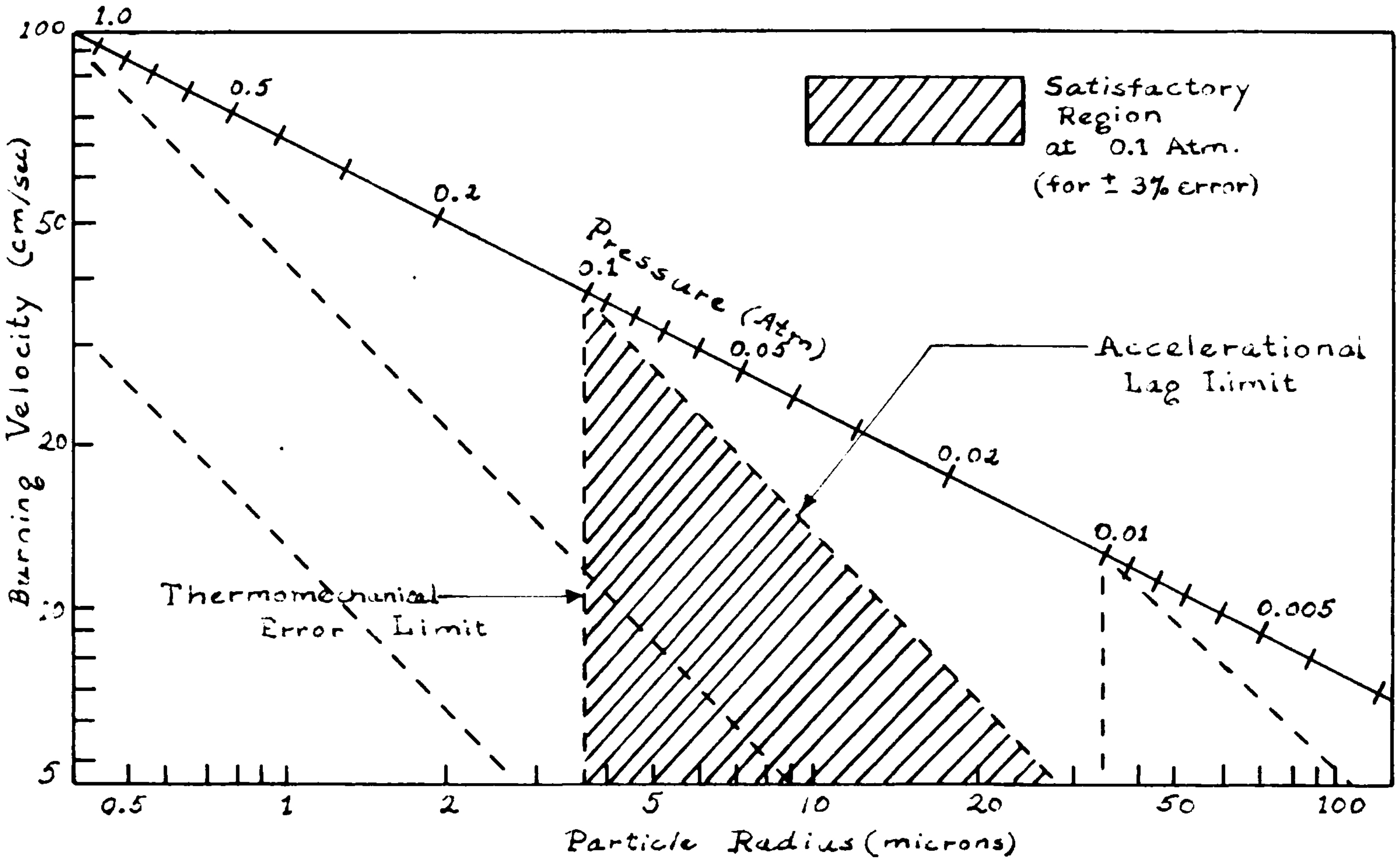

Figure 1.6 Range of Application of Particle Track Technique (Ref. 7)

outline the region for any other pressure, locate the pressure on the diagonal axis. From this point drop a normal to the particle radius abscissa and run a line parallel to the dashed diagonal lines (pressure diagonals). The enclosed area formed by the above procedure shows the range of applicability.

CHAPTER II

DESCRIPTION OF APPARATUS

A. Construction of Burner

Figure 2.1 shows schematically the construction of the flat flame burner which was utilized in carrying out the experiments and which is very similar to the one used by Botha and Spalding. This direct cooling burner is constructed of brass and consists of a main burner tube with an inner diameter of two inches, containing four 1/8 inch thick sintered porous bronze discs at its exit end. The selection of the porosity and number of the bronze discs is considered to be extremely critical, since the type and number of discs determines the pressure drop of the mixture flow across the discs and helps to insure laminar flow. In the case of this flat flame burner, a filter porosity was selected that would allow passage of particles no larger than 15 microns in diameter. The cylindrical surfaces of the top and bottom discs are burnished to provide smooth edges prior to installation of the discs into the burner housing. Furthermore, the inside surface of the two inch diameter brass tube is machined at the upper end to provide a leading surface in the burner housing for insertion of the porous discs. The discs are

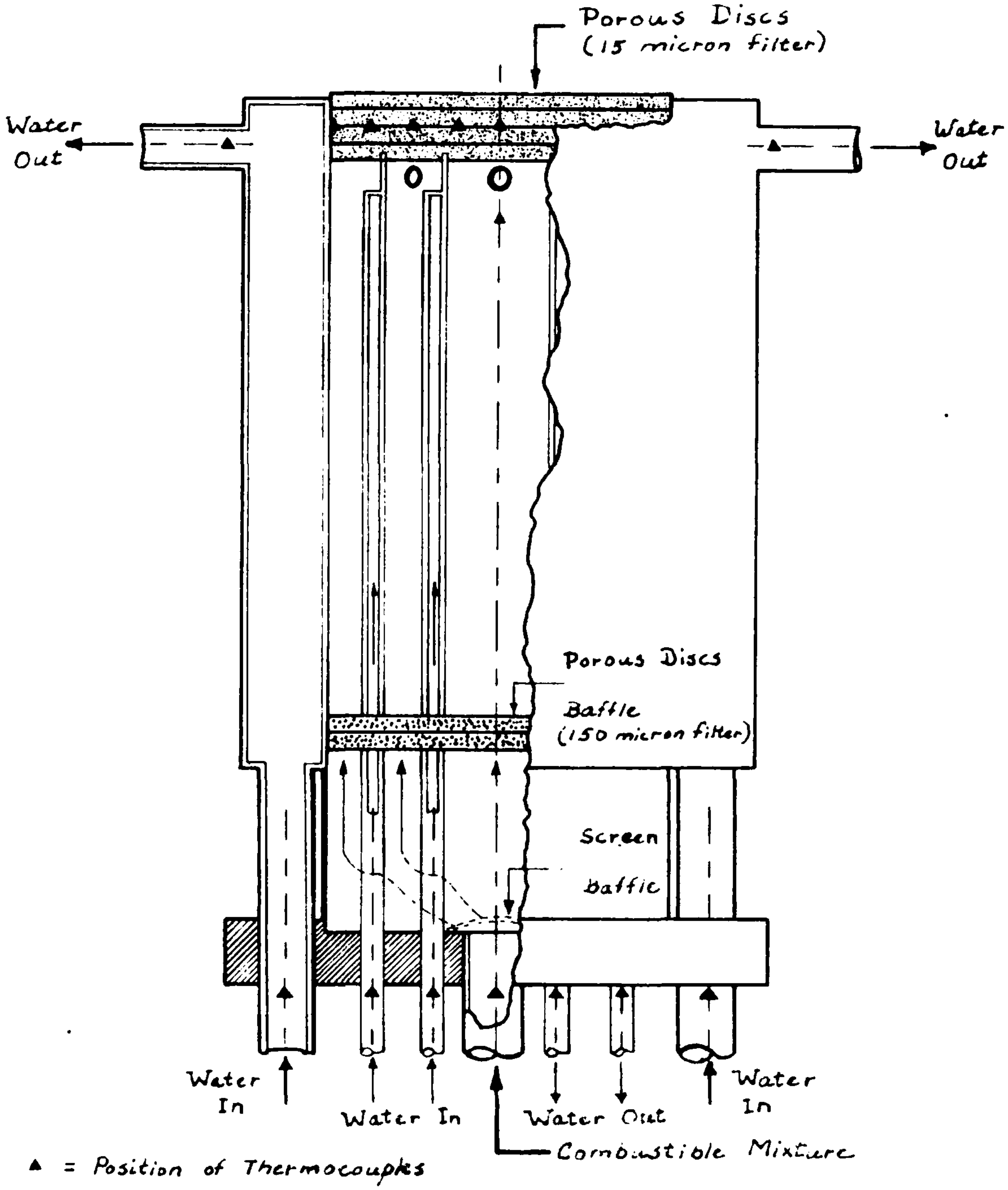

Figure 2.1 Two Inch Diameter Flat Flame Burner with Concentric Water Jackets

then fitted into the burner housing with the use of an hydraulic press; the net result is the establishment of a good thermal contact between the discs and the inner wall of the brass tube which contains a water-cooling system. In addition, it should be apparent that a temperature gradient would exist from the outside rim of the discs to the center if there was simply an outer water-cooling jacket. This is because the heat conducted to the discs by the combustion process would be carried away at only the outside edges through the two inch diameter brass tube to the cooling water. Consequently, in order to obtain more uniform conditions and a greater degree of accuracy, heat is also conducted away from the discs at two other radii by means of two additional concentric, cylindrical water jackets inside the main burner tube. The stream of cooling water through each of the water jackets is divided in two and guided by a spiral vane to prevent the formation of pockets of hot water. The water-cooling jackets extend over nearly the entire length of the burner tube with water inlets and outlets at the bottom for the two inner water jackets and water inlets at the bottom and outlets at the top for the outermost cooling jacket. The burner tube is soldered to a base disc made of solid brass through which the air/fuel mixture passes. The air/fuel mixture is immediately diffused by a wire screen baffle placed directly above the mixture inlet. The mixture then proceeds up the burner tubing through two 150 micron filters which assist in further diffusing the mixture and insuring that a uniform velocity is achieved as the mixture passes around the concentric water-cooling jackets.

The mixture stream reaches the bottommost 15 micron porous disc in a relatively uniform condition. Small perforations in the top of the two inner concentric cooling jackets also assist in insuring an equal distribution of mixture pressure. The stream then penetrates through the four layers of 15 micron sintered bronze and appears above the top disc with a uniform velocity over the entire cross-sectional area. When the stream speed is less than the adiabatic flame speed for a certain mixture of fuel and air, combustion takes place in the form of a flat flame front a small distance above the top disc.

It was pointed out above that some of the heat transferred by the flame to the disc is carried away from the outside edges through the brass tube to the cooling water. The remainder of the heat is extracted through the use of two inner, concentric cylindrical water jackets firmly embedded at the top in the fourth 15 micron porous disc as is shown in Figure 2.1. This arrangement of cooling jackets is very satisfactory and is paramount in maintaining a zero temperature gradient radially across the porous discs. Maintenance of a zero radial temperature gradient helps to make the flame burn flat.

Copper-constantan thermocouples were placed at five different radii in the second disc from the top as shown in Figure 2.1 in order to measure the temperature distribution in the discs.

The inlet and outlet water temperatures, as well as the temperature of the air/fuel mixture inside the burner are also measured by copper-constantan thermocouples. The overall dimensions of the burner are 8-1/2 inches in height and 3-1/4 inches in diameter.

B. Arrangement of Equipment

Figure 2.2 shows schematically the arrangement of the apparatus. Air from a receiver tank (A) maintained at 125 psig is delivered through two needle valves (B) via 1/4 inch copper tubing into a 250 ml pyrex glass drying tower (C) containing calcium chloride for drying the air. The air then passes through a Fischer-Porter variable-area flowmeter (E), enters a copper tube tee-fitting (F) and is subsequently mixed with propane in a glass-wool filled mixing chamber (G). The propane follows a similar path from a different source consisting of a bottle of liquified propane (H), valves (I), drying tower (J), and flowmeter (K).

From the mixing chamber (G) the mixture now may flow either through a particle injection system consisting of a one liter pyrex three-neck distillation flask (L)

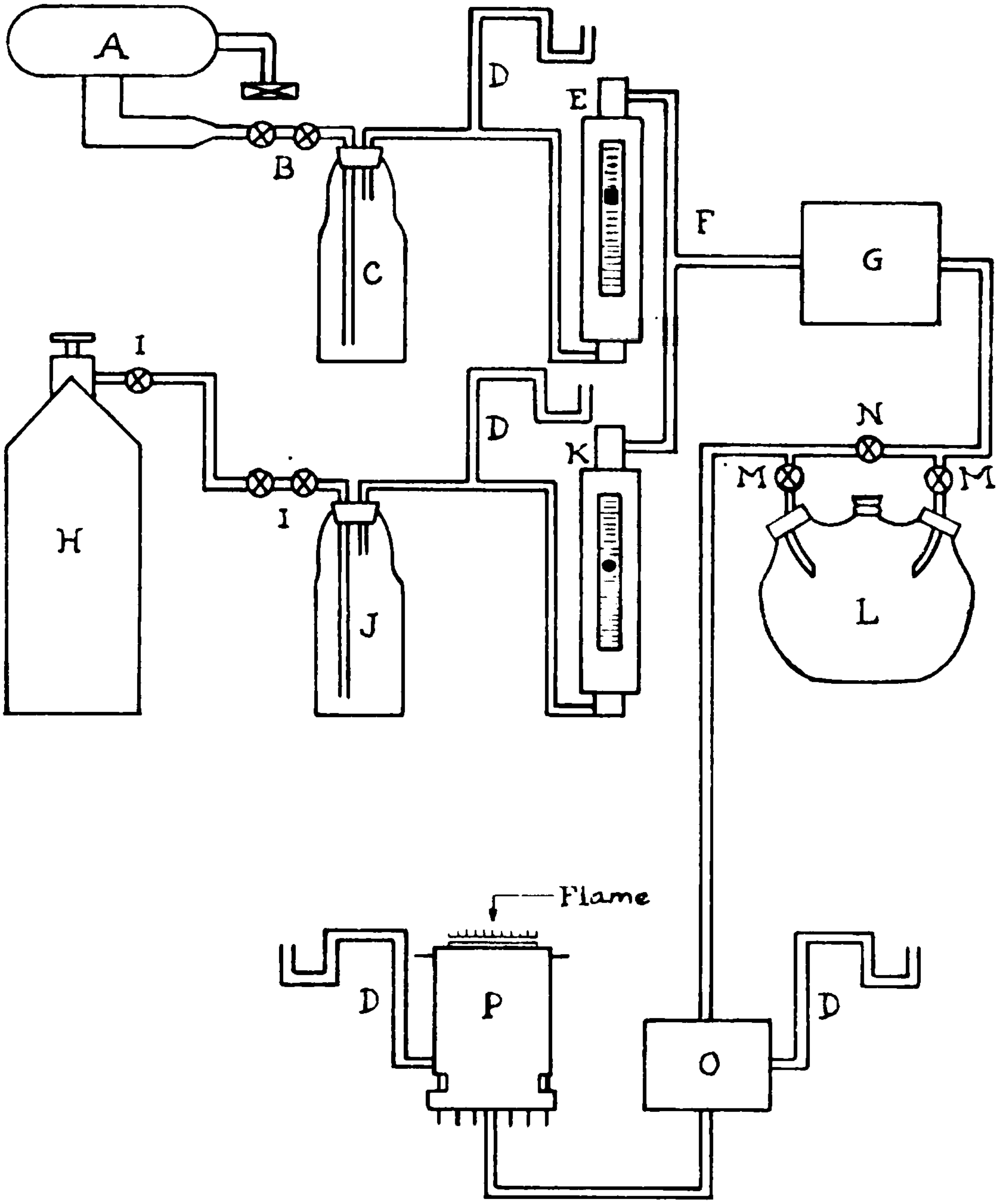

Figure 2.2 Schematic of Equipment for Burner System

containing magnesium oxide dust or, with inlet and outlet valves (M) closed and a parallel needle valve (N) open, the particle injection system is by-passed. The mixture, with or without particles, then proceeds through a 150 micron filter and a 15 micron filter (O) which together serve to size the particles and eliminate those which will not be able to penetrate the 2 inch diameter porous disc of the burner. The fuel mixture then passes into the base of the burner (P). Pressure and temperature measurements may be taken by means of manometers (D) at different points in the flow system in order to apply corrections for changes in volume due to local pressure and temperature changes.

The burner was dimensioned to conform to the University of Arizona combustion tunnel, the details of which are contained in Pyle's thesis (22). The tunnel consists of a 3-1/2 inch diameter nozzle enclosed by an 18 by 18 inch stack as shown in Figure 2.3. The burner is inserted into the nozzle of the tunnel and may be adjusted to the proper height to adapt to existing photographic facilities, in particular the particle track equipment. The combustion tunnel contains glass windows on three sides which serve the twofold purpose of providing photographic access to the flame during experimentation and also protection against outside drafts. Additional equipment outside the stack of the tunnel consists of schlieren mirrors, particle track facilities, and related photographic

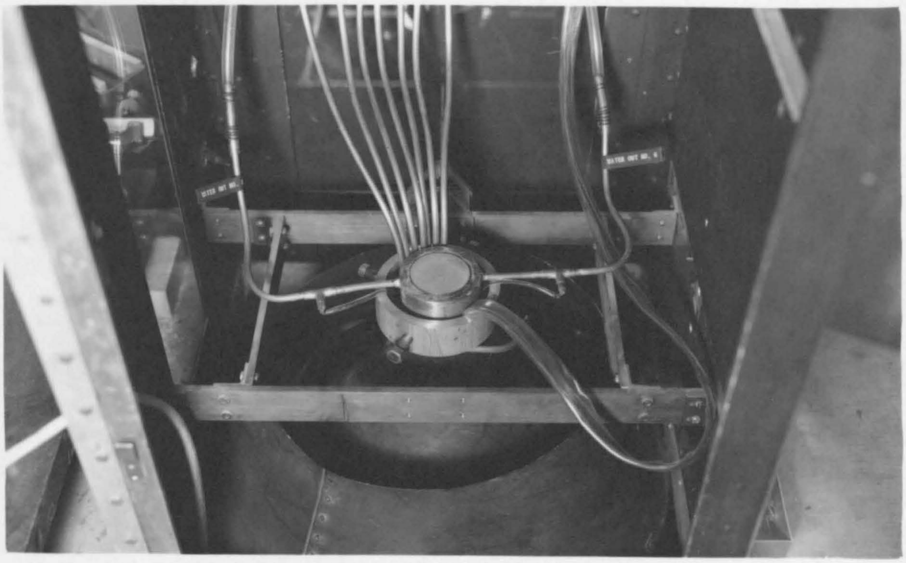

Figure 2.3 Burner Mounted in Combustion Tunnel

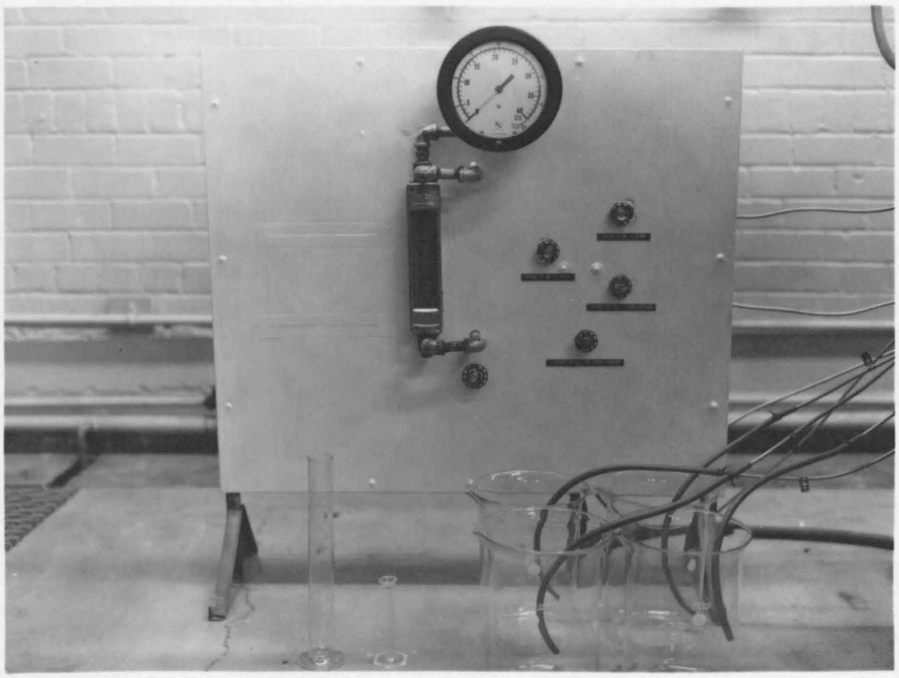

Figure 2.4 Cooling Water System Control Panel

equipment. Air/fuel lines, pressure taps, water lines, and thermocouple wiring were passed around the outside of the burner housing near the top edge of the nozzle and inserted through a 1/4 inch thick aluminum panel located 4 feet above the burner port.

C. Method of Measurement

The cooling water used was local city water, which flowed through a control panel as shown in Figure 2.4. The total passage of water and the flow rate through each water jacket was monitored at this control panel, and once the flow rates in the different water jackets had been established as required, they were kept constant throughout a series of experiments.

Cooling baths, as shown in Figure 2.5, were filled with isopropyl alcohol and ice thereby insuring that the water entering the burner cooling jackets was of the appropriate temperature. Also, a Leeds and Northrup potentiometer of high sensitivity and a multi-position thermocouple switch with a cold junction made it possible to swiftly and accurately measure an electromotive force down to 0.001 of a millivolt. The corresponding temperature equivalent was accurate to 1/20 of a degree Fahrenheit for copper-constantan.

Since the air and propane are available at pressures greater than that required for the burner, the

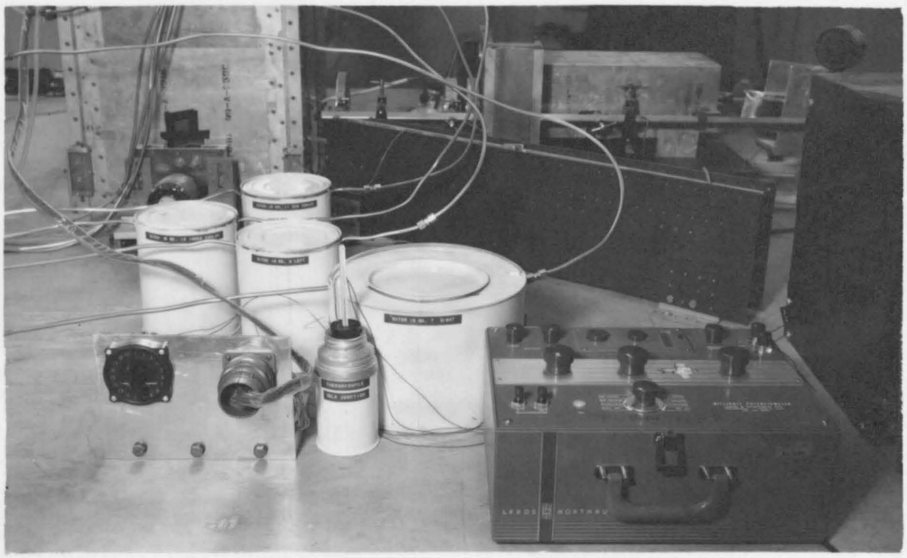

Figure 2.5 Potentiometer, Thermocouple Junction, and Cooling Baths

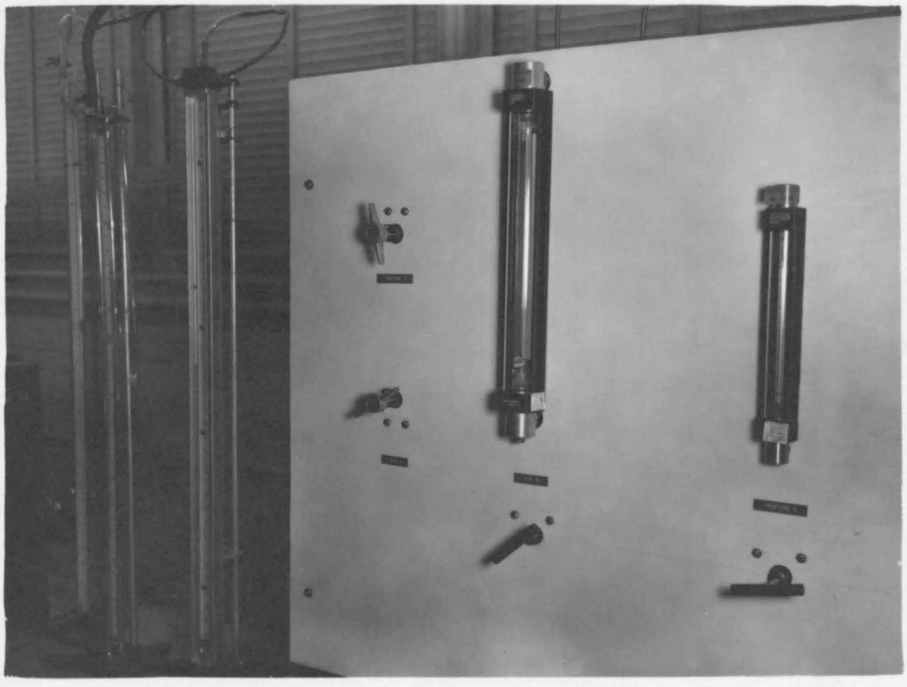

Figure 2.6 Air/Fuel System Control Panel

pressure is reduced through the use of a series of needle valves of high quality. Both the air and propane are dried in calcium chloride drying towers and are considered to be applied in a dry state to the burner.

Mercury manometers are placed immediately upstream of the propane and air flowmeters as shown in Figures 2.2 (D) and 2.6. The Fischer-Porter variable-area flowmeters have been factory calibrated for propane and air respectively at standard conditions of 14.7 psia and 70°F. The air meter has a maximum flow capacity of 1.12 cfm of air at 14.7 psia and 70°F and is read in per cent of total flow at standard conditions. The propane meter is of the tri-flat tube variety with a maximum flow rate of 1800 cc/min of propane at full scale reading and 14.7 psia and 70°F. Scale readings are referenced to chart data and are based on the ratio of the tube diameter to float diameter.

It can be easily shown that the deflection of the float is such that the drag on the float equals the weight which is a constant. Under standard conditions, the following relationship yields

$$\rho_m V_m^2 A_f = \rho_s V_s^2 A_f \tag{2.1}$$

where ρ_m is the density of the fluid at the meter, V_m is the velocity of the fluid at the meter, A_f is the effective frontal area of the meter float, ρ_s is the density under standard conditions, and V_s is the velocity at standard conditions. Thus it follows that

$$\rho_s V_s^2 = \text{Constant} = B^2 \tag{2.2}$$

$$V_s = \frac{B}{\sqrt{\rho_s}} \tag{2.3}$$

Also, the volumetric flow rate ($\dot{I}\dot{F}$) under standard conditions is stated by

$$\dot{I}\dot{F} = A V_s = \frac{A B}{\sqrt{\rho_s}} , \tag{2.4}$$

where A is the effective flow area at the flowmeter. Furthermore, the mass flow rate at non-standard conditions is

$$\dot{m} = \rho_m A V_m \tag{2.5}$$

where

$$V_m = \frac{B}{\sqrt{\rho_m}} \tag{2.6}$$

or

$$\dot{m} = \rho_m \frac{A B}{\sqrt{\rho_m}} . \tag{2.7}$$

However

$$A B = \sqrt{\rho_s} (I F) \tag{2.8}$$

and

$$\dot{m} = \rho_m \sqrt{\frac{\rho_s}{\rho_m}}\,(I\ F) = \rho_s \sqrt{\frac{\rho_m}{\rho_s}}\,(I\ F). \qquad (2.9)$$

The mass flow rate is then expressed as

$$\dot{m} = \rho_s \sqrt{\frac{P_m}{P_s}\ \frac{T_s}{T_m}}\,(I\ F) \qquad (2.10)$$

When determining an air to fuel ratio by weight the following two expressions are utilized:

$$\dot{m}\ (air) = \rho_s\ (air) \sqrt{\frac{P_m(air)}{P_s}\ \frac{T_s}{T_m(air)}}\,(I\ F)(air) \qquad (2.11)$$

$$\dot{m}\ (fuel) = \rho_s\ (fuel) \sqrt{\frac{P_m(fuel)}{P_s}\ \frac{T_s}{T_m(fuel)}}$$

$$\sqrt{\frac{M\ (air)}{M\ (fuel)}}\,(I\ F)(fuel) \qquad (2.12)$$

where M is the molecular weight of either the air or the fuel (propane), and the following relationship follows from the above conditions.

$$A/F = \sqrt{\frac{M\ (air)}{M\ (fuel)}\ \frac{P_m(air)}{P_m(fuel)}\ \frac{T_m(fuel)}{T_m(air)}}\ \frac{(I\ F)(air)}{(I\ F)(fuel)} \qquad (2.13)$$

The calculation for flame speed requires the computation of a total mass flow rate given by

$$\dot{m}\ (nozzle\ of\ burner) = \dot{m}\ (air) + \dot{m}\ (fuel), \qquad (2.14)$$

which suggests

$$\rho_n\ A_n\ V_n = \rho_s(\text{air}) \sqrt{\frac{P_m(\text{air})}{P_s} \quad \frac{T_s}{T_m(\text{air})}}\ (\text{I F})(\text{air})$$

$$+\rho_s(\text{fuel}) \sqrt{\frac{P_m(\text{fuel})}{P_s} \quad \frac{T_s}{T_m(\text{fuel})} \quad \frac{M\ (\text{air})}{M\ (\text{fuel})}}\ (\text{I F})(\text{fuel}) \qquad (2.15)$$

where the subscript n designates conditions at the flame front. It also follows that

$$A_n\ V_n = \frac{P_s\ R_n\ T_n}{R\ (\text{air})\ T_s\ P_n} \sqrt{\frac{P_m(\text{air})}{P_s}}\ (\text{I F})(\text{air})$$

$$+ \frac{P_s\ R_n\ T_n}{R\ (\text{fuel})\ T_s\ P_n} \sqrt{\frac{P_m(\text{fuel})}{P_s} \quad \frac{M\ (\text{air})}{M\ (\text{fuel})}}\ (\text{I F})(\text{fuel}) \qquad (2.16)$$

where

$$R_n = \frac{\dot{m}\ (\text{air})\ R\ (\text{air}) + \dot{m}\ (\text{fuel})\ R\ (\text{fuel})}{\dot{m}\ (\text{nozzle of burner})}$$

$$= \frac{\left[\dot{m}\ (\text{air}) + \dot{m}\ (\text{fuel})\ \frac{M\ (\text{air})}{M\ (\text{fuel})}\right] R\ (\text{air})}{\dot{m}\ (\text{air}) + \dot{m}\ (\text{fuel})} \qquad (2.17)$$

and the flame speed is then given by the equation

$$V = \frac{P_s\ T_n\ R_n}{A_n\ P_n\ T_s\ R\ (\text{air})} \left[\sqrt{\frac{P_m(\text{air})}{P_s}}\ (\text{I F})(\text{air}) + \sqrt{\frac{M\ (\text{fuel})}{M\ (\text{air})} \quad \frac{P_m(\text{fuel})}{P_s}}\ (\text{I F})(\text{fuel})\right] \qquad (2.18)$$

Calculations of the total amount of heat, Q, absorbed by the cooling water jackets in Btu/lbm of propane are obtained by dividing the rate of heat extraction via the water jackets by the mass rate of flow of propane as given in equation 2.12, where the air/fuel mixture entering the burner is at 79° $\pm$ .5°F and at atmospheric pressure.

The calculations of the data are presented in section B of Chapter III.

CHAPTER III

EXPERIMENTAL PROCEDURE

A. Operation of Burner

Initial operation of the flat flame burner system revealed that satisfactory performance characteristics could be achieved throughout a wide range of flame speeds. Figure 3.1 displays the characteristic flat flame burning a short distance above the burner's top porous disc.

For each series of experiments the air/fuel mixture ratio was varied from the lower to the upper limit of combustion while the total flow rate of the air/fuel mixture was kept practically constant. The air/fuel ratio was altered by decreasing the fuel rate and at the same time increasing the air rate to maintain a nearly constant overall flow rate. Each one of the series of experiments is begun by igniting a rich mixture (air/fuel ratio approximately equal to 7) which assures that the burning rate will slightly exceed the flow rate causing the flame to be attached to the surface of the porous plug. The mixture is then adjusted until a "semi-diffusion flame" appears on top of the burner. This flame is described in detail in section B of this chapter. Then, while decreasing the fuel flow rate and increasing the air flow rate, the flame

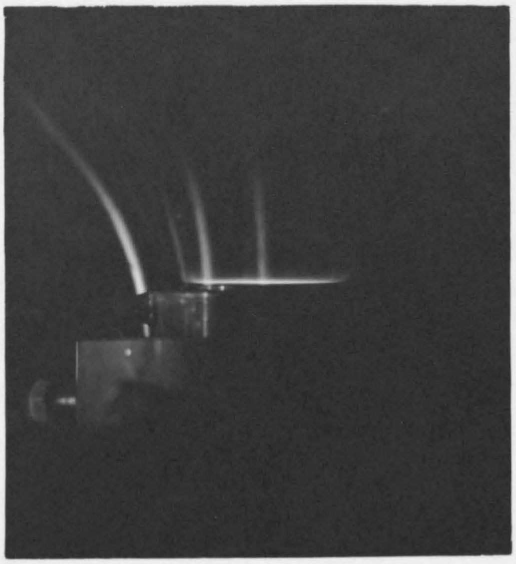

Figure 3.1 Characteristic Flat Flame; V_u = 0.607 ft/sec, A/F = 15.6, Q = 2420 Btu/lbm

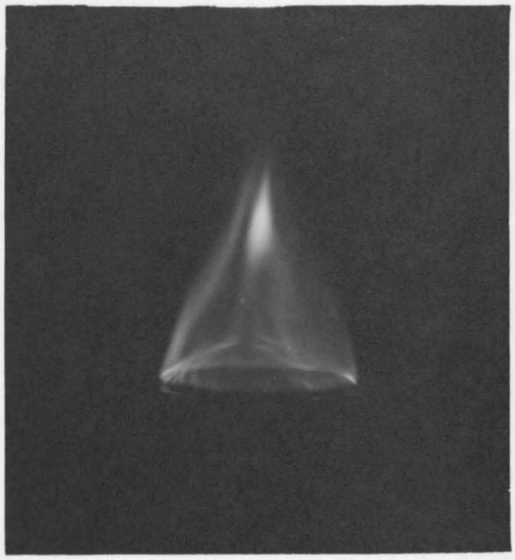

Figure 3.2 Semi-diffusion Flame on Top of Flat Flame Burner; V_u = 0.484 ft/sec, A/F = 8.79, Q = 484 Btu/lbm

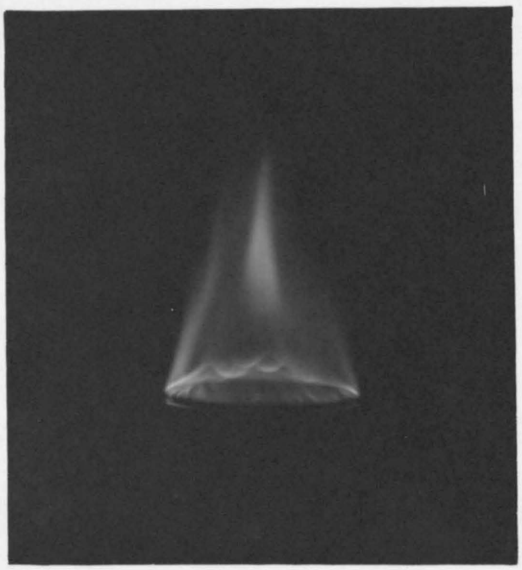

Figure 3.3 Initial Cell Formation; V_u = 0.485 ft/sec, A/F = 9.10, Q = 581 Btu/lbm

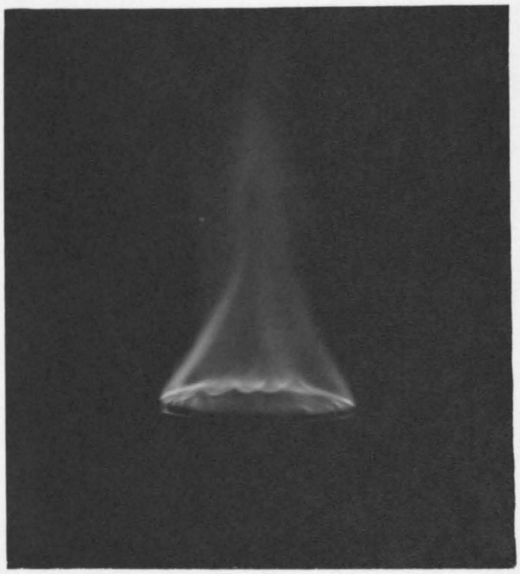

Figure 3.4 Isolation of Cells by Non-luminous Ridges; V_u = 0.485 ft/sec, A/F = 9.15, Q = 607 Btu/lbm

eventually becomes almost perfectly flat. The following readings are recorded for each air/fuel ratio during a specific series: the pressure at the flowmeters; the pressures at the outlets of both flowmeters; the temperatures of the propane and air at the flowmeters; the pressure inside the burner; the temperatures at five different radii in the second porous disc of the burner; the inlet and outlet temperatures of the cooling water through each water jacket; the rates of flow of cooling water through each water jacket; the temperature inside the burner immediately prior to entering the 15 micron porous plugs; and the atmospheric temperature and pressure.

After every adjustment of air/fuel ratio, at least five minutes are allowed for conditions to stabilize. When the upper limit of the air/fuel ratio is reached, the flame is finally blown off. The mixture flow rate is then readjusted and a new series of readings is taken. The air/fuel mixture ratios investigated covered the entire range from a lower limit of about 7.00 to an upper limit of about 30.00. Total mixture flow speeds varied from 0.099 ft/sec. to 1.495 ft/sec.* The area of the flame was determined photographically.

*The reason for computing values of flame speed and air/fuel ratio to four significant digits is because a difference in flame characteristics is discernible to the fourth figure, however no claim is made as to the magnitude of the accuracy at the fourth digit.

The adaptability of the burner for particle track studies was verified by injecting magnesium oxide dust into the burner system at various air/fuel ratios. During particle injection the color of the flame changed from a light blue to a bright orange. This was evidence that magnesium oxide particles were entering the flame. However, photographs taken simultaneously with particle injection failed to produce visible traces of the particles. It is felt that what is necessary for satisfactory particle track photography is a significant improvement in the stroboscopic illumination. This is discussed in detail in Kaser's dissertation (13). After four hours of operation with mixtures containing magnesium oxide dust, the 15 micron filter that was installed upstream of the burner began to clog and the flow became restricted necessitating discontinuance of particle injection.

B. Test Results

The quantities obtained from the measurements are (1) the total amount of heat carried away by the cooling water expressed as Q, Btu per lbm of propane, where the propane is measured at 79° $\pm$ .5°F and atmospheric pressure, (2) the air/fuel ratio, A/F, expressed as lbm of air per lbm of propane, and (3) the speed of the air/fuel mixture entering the flame expressed in ft/sec.

A typical series yielded the following experimental observations which are plotted as curve number 3 on Figure 3.17. Curve number 3 represents a mixture speed of 0.502 $\pm$ 0.018 feet per second and afforded the following observations concerning flame structure:

1. When initially a very rich mixture is ignited with an air/fuel ratio of about 7.05, combustion takes place in the form of a large and irregularly shaped "semi-diffusion flame" with a yellow tail and inner cone, much the same as that of a Bunsen flame. The "semi-diffusion flame," which consists of the air and the fuel reacting at an interface, appears in a very interesting configuration in the case of the flat flame burner. Within the "semi-diffusion flame," the angle between the sides of the inner cone and the porous disc is very small. This occurrence is shown in Figure 3.2 for an air/fuel ratio of 8.79.
2. As the air/fuel ratio is increased to 9.10, the inner cone begins to break down to form a number of individual cells, hemispherical in appearance, which are convex toward the unburned gas mixture. This occurrence is clearly shown by Figure 3.3.
3. When the air/fuel ratio is increased to 9.15 the cells start to become sharply isolated from each other by non-luminous or dark ridge lines within

the flame as shown in Figure 3.4. The cells are then arranged irregularly about a central cell.

4. Upon increasing the air/fuel ratio, the number of cells increases while their diameter decreases as shown in Figure 3.5.
5. Increasing the air/fuel ratio to 10.31 results in the upper tips of the individual cells joining to form a continuous corrugated flame front, as is shown in Figure 3.6.
6. As the air/fuel ratio is increased from 10.31 to 11.26 the flame front corrugation slowly flattens out until an air/fuel ratio of 11.26 is achieved. Figure 3.7 shows this gradual flattening out of the sharp tips at an air/fuel ratio of 10.76.
7. At an air/fuel ratio of 11.26 the flame front becomes almost perfectly flat as shown by Figure 3.8.
8. The flame front remains flat for further increases in mixture ratio until an air/fuel ratio of 25.56 is reached, when again the flame starts to become distorted by forming a slight buckling ridge in the center of the disc as is shown in Figure 3.9. This buckling or distortion is concave toward the unburned gas and the edges of the flame sheet start to appear wrinkled and frayed.
9. Wrinkling becomes more severe at an air/fuel ratio of 28.47 as is shown in Figure 3.10.

Figure 3.5 Number of Cells Increases; V_u = 0.487 ft/sec, A/F = 10.20, Q = 753 Btu/lbm

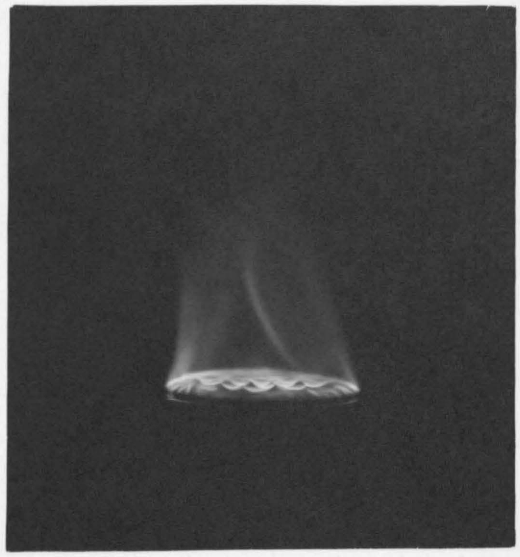

Figure 3.6 Individual Cells Join at Their Tips; V_u = 0.488 ft/sec, A/F = 10.31, Q = 780 Btu/lbm

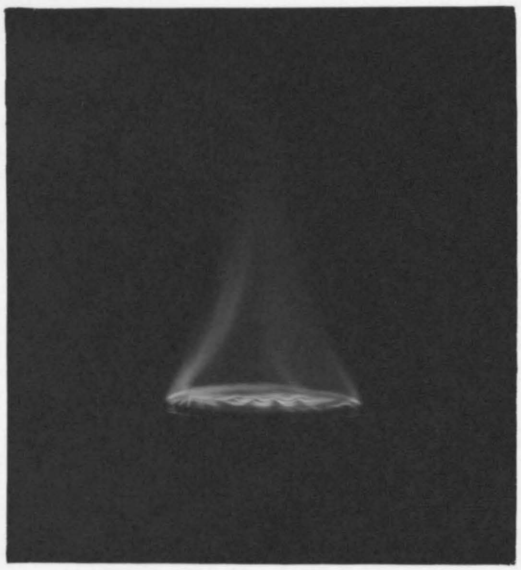

Figure 3.7 Flattening Out of Flame Front; V_u = 0.490 ft/sec, A/F = 10.76, Q = 907 Btu/lbm

Figure 3.8 Flat Flame Front V_u = 0.495 ft/sec, A/F = 11.26, Q = 1017 Btu/lbm

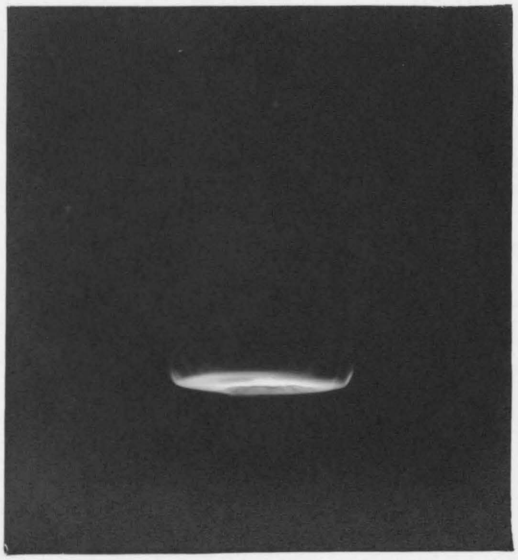

Figure 3.9 Initial Buckling and Frayed Edges; V_u = 0.503 ft/sec, A/F = 25.56, Q = 434 Btu/lbm

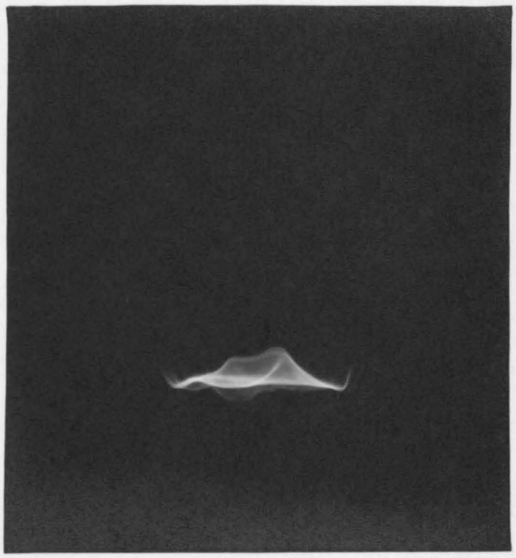

Figure 3.10 Rigid Distortion Near Blow-off; V_u = 0.504 ft/sec, A/F = 28.47, Q = 289 Btu/lbm

Figure 3.11 Blow-off; V_u = 0.506 ft/sec, A/F = 29.13, Q = 222 Btu/lbm

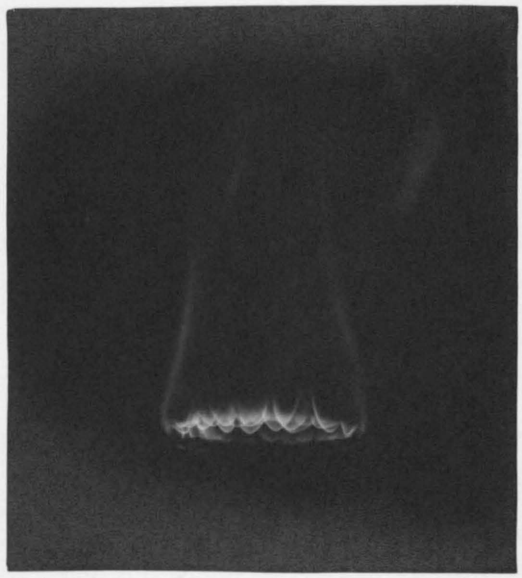

Figure 3.12 Formation of High Dark Ridges Between Cells; V_u = 1.495 ft/sec, A/F = 10.05, Q = 193 Btu/lbm

10. The flame is ultimately blown off in a distorted form at an air/fuel ratio of 29.13 as is pictured in Figure 3.11.

In Figure 3.17, curve number 9 represents a mixture speed of approximately 1.495 feet per second. The following observations are made with respect to curve number 9, Figure 3.17:

1. For air/fuel mixture ratios of 8.98 and lower, combustion takes place in the form of a "semi-diffusion flame" as described before.
2. As the air/fuel ratio is increased, the flame forms an increasing number of cells, any number of which may be stabilized. While the number of cells increases, their diameter decreases between air/fuel ratios of 9.13 and 10.45.
3. At an air/fuel ratio of 10.05, the dark ridges between the cells become extremely high and occasionally erupt emitting vertical streaks or bands of yellow radiation which are clearly observed with the naked eye, but which were never obtained photographically. These yellow bands have been attributed to the formation of pockets of carbon. Figure 3.12 attempts to show the phenomenon of the formation of the high dark ridges between the cells.

4. Upon increasing the air/fuel ratio from 10.45 to 13.91, more and more cells form covering the entire disc. Up to an air/fuel ratio of about 13.91 the cells are still isolated from each other by the non-luminous ridges mentioned previously. A typical photograph for this case is shown in Figure 3.13. Although the non-luminous ridges are clearly observable visually, it is rather difficult to detect their presence in the photograph.
5. At an air/fuel ratio of 14.09 the non-luminous ridges disappear and the edges of the cells completely join to form a continuously corrugated flame front as is shown in Figure 3.14.
6. As the air/fuel ratio approaches stoichiometric, the color of the cells changes from blue green to blue violet and when increasing the mixture ratio beyond 15.6 the corrugated flame front becomes distorted. Once again the distortion is concave towards the unburned gases. The flame then begins to lift slowly from the disc and is ultimately blown off at an air/fuel ratio of about 27.84. Thus, in summary, a smooth flat flame was never observed when the mixture speed reached the value of 1.495 feet per second.

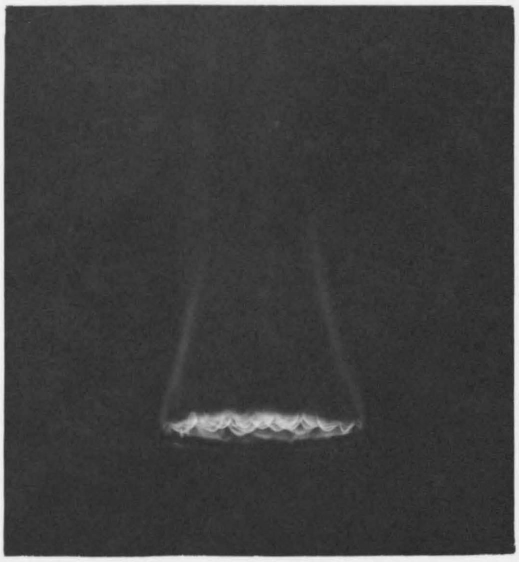

Figure 3.13 Non-luminous Ridges Start to Decay; V_u = 1.497 ft/sec, A/F = 13.91, Q = 289 Btu/lbm

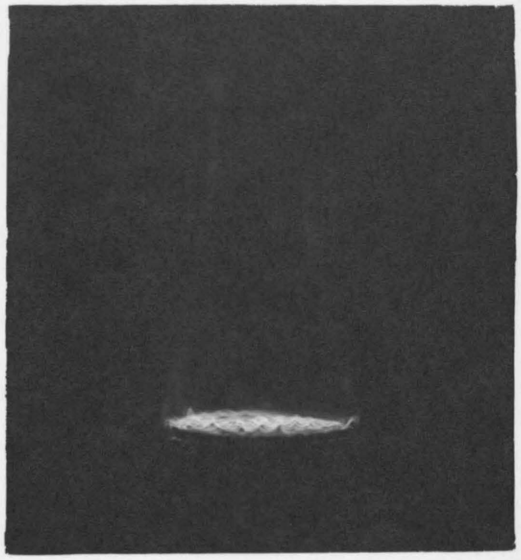

Figure 3.14 Continuous Corrugated Flame Front; V_u = 1.498 ft/sec, A/F = 14.09, Q = 308 Btu/lbm

Figure 3.15 Formation of Concentric Ring or Wave; V_u = 0.130 ft/sec, A/F = 8.10, Q = 1350 Btu/lbm

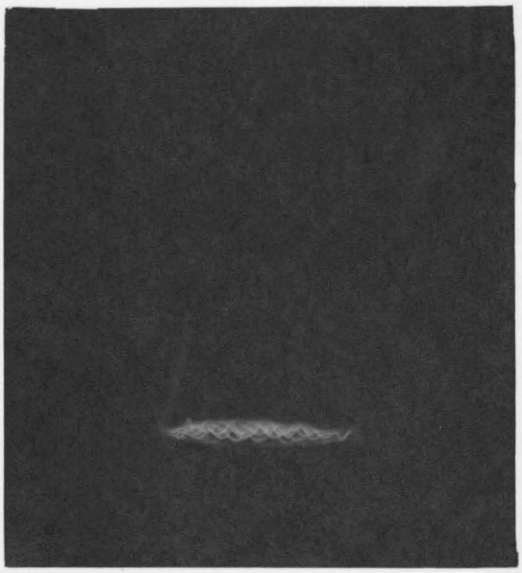

Figure 3.16 Tight, Non-Concentric Packing at High Flow Speeds; V_u = 1.330 ft/sec, A/F = 13.80, Q = 309 Btu/lbm

Another very interesting phenomenon occurs at very low mixture speeds of less than 0.130 feet/sec. Under the appropriate conditions of air/fuel ratios not only do the cells begin to join together, but they form a perfectly concentric ring of six cells around a center cell and when viewed from the top of the burner, the ring of cells tends to rotate, sometimes in the clockwise and other times in the counterclockwise direction. Figure 3.15 attempts to show the formation of the concentric ring but due to the lack of depth of field obtainable with the camera and limitations of the viewing angle, the connecting cells in the rear were not clearly photographed.

One of the characteristics of cellular formation which should be noted is the variance in packing arrangement at the higher flame speeds. This is clearly depicted by the very tight, nonconcentric packing at the higher flow speed of 1.330 feet/second as is shown in Figure 3.16. The air/fuel ratio in this Figure is 13.80.

C. Discussion of Test Results

In Figure 3.17 is shown a series of curves representing lines of approximately constant mixture speeds plotted on the basis of heat carried away in Btu/lbm of propane versus air/fuel ratio by weight. These curves represent the results of the experimental data obtained. The values of the mixture speeds for the different curves

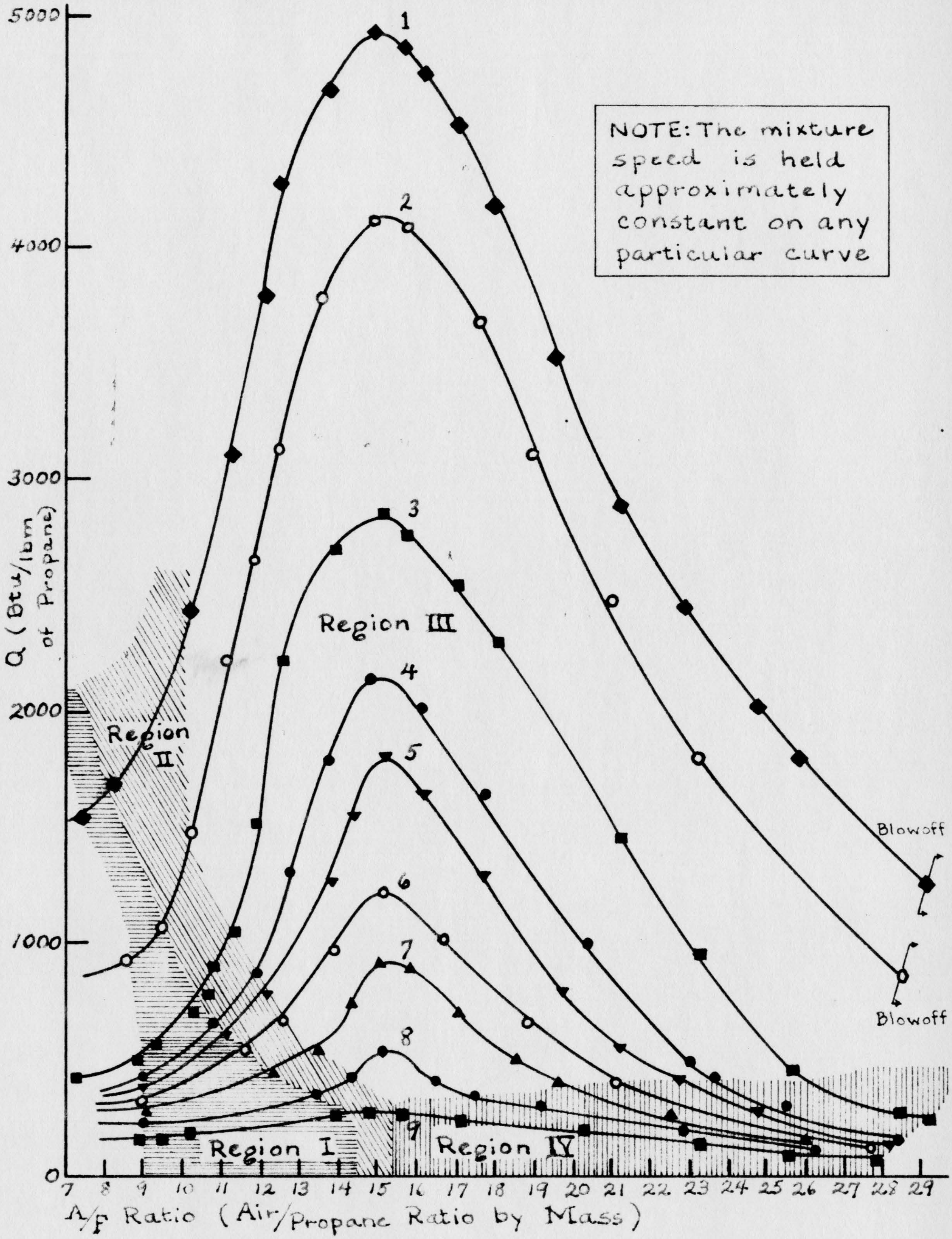

Figure 3.17 Heat Carried Away Versus Air/Fuel Ratio for Different Mixture Speeds

at an air/fuel ratio of 14.95 are shown in Figure 3.18. These speeds are the experimental values obtained with a small amount of variation. The maximum variation obtained is approximately equal to 0.018 feet per second on either side of the value at the stoichiometric air/fuel ratio. It should be noted that exact experimental data obtained for each series were used to compute the points on the chart of Figure 3.17 and not the average value from any series of tests.

The maximum of all the curves in Figure 3.17 appears at or near a mixture ratio of 14.95 which is slightly richer than a stoichiometric mixture of 15.60.

Figure 3.17 is sectioned into four separate regions. Region I is the leftmost cross-hatched area and the left margin of this region marks the points at which the "semi-diffusion flame" starts to disappear and initially form cells which are isolated from each other by non-luminous ridges. The right-hand boundary of region I marks the points at which the non-luminous ridges disappear and the individual cells join to form a continuous corrugated surface. Moving laterally to the right through region II the corrugations begin to flatten out until the right hand margin of region II is reached where the flame front becomes perfectly flat. Throughout region III, which is the noncross-hatched area, the flame front remains flat. Those locations where the right hand margin of region III

Curve Number	Mixture Speed in Feet per Second (V_u)
1	0.099 feet/second
2	0.173 feet/second
3	0.502 feet/second
4	0.723 feet/second
5	0.830 feet/second
6	1.015 feet/second
7	1.120 feet/second
8	1.231 feet/second
9	1.495 feet/second

Figure 3.18 Values of Mixture Speed for the Curves of Figure 3.17 at an Air/Fuel Ratio of 14.95

does not come into contact with a cross-hatched area are intended to indicate that the flame immediately proceeded from a flat configuration to blow off with no distortion. Region IV is that area where the flame changes from a flat front or a corrugated front to a distorted or rigid cellular structure, the cells being concave toward the unburned gas. The right hand margin of region IV is where the flame is ultimately blown off in a distorted configuration.

Although it appears from Figure 3.17 that the curves end at mixture ratios of approximately 7.00, this is not strictly true since mixtures richer than 7.00 are obtainable. In this particular case combustion appears to take place in the form of a long and irregularly shaped flame with a yellow tail extending almost the entire length of the flame.

It should also be noted in Figure 3.17 that only in the flat flame region, region III, does the mixture speed equal the flame speed. Inside the cross-hatched areas, the mixture speed is not related to the true flame speed, since in these distorted regions the flame front becomes inclined to the stream velocity. It is therefore obvious that in the distorted or cellular regions the "flame speeds," calculated by dividing the measured mixture flow rate by the "area," were too large since the true area was considerably larger. This explains, to some extent, the leveling out of the curves in the cellular, corrugated, or distorted regions.

The effects of heat extraction from the flame are shown in Figures 3.19 and 3.20 which are plots of flame speed versus heat extracted with air/fuel as a parameter. Figure 3.19 is for values of air/fuel ratios equal to or greater than 14.95 and Figure 3.20 is for air/fuel ratios equal to or less than 14.95. From these two graphs it is evident that flame speed is linearly decreasing with Q (the heat carried away by the cooling water) for a constant air/fuel mixture over a fairly wide range of air/fuel ratios. Once again the flat flame regions in Figures 3.19 and 3.20 are those outside the cross-hatched areas. The cross-hatched areas represent regions where the flames are wrinkled, cellular, or distorted. Extrapolation of the linear portion of any given curve to the vertical flame speed axis determines the adiabatic flame speed (at a temperature of 79 $\pm$ .5°F) for a particular air/fuel ratio which is held constant for the given curve. In these two Figures the distorted or cellular region makes the extrapolation of the lines difficult and uncertain for the high and low values of air/fuel ratios such as 23.20 and 12.00 because of the short interval of Q over which the flat flame persists. However, for values intermediate to these there can be little doubt as to the validity of the linear extrapolation.

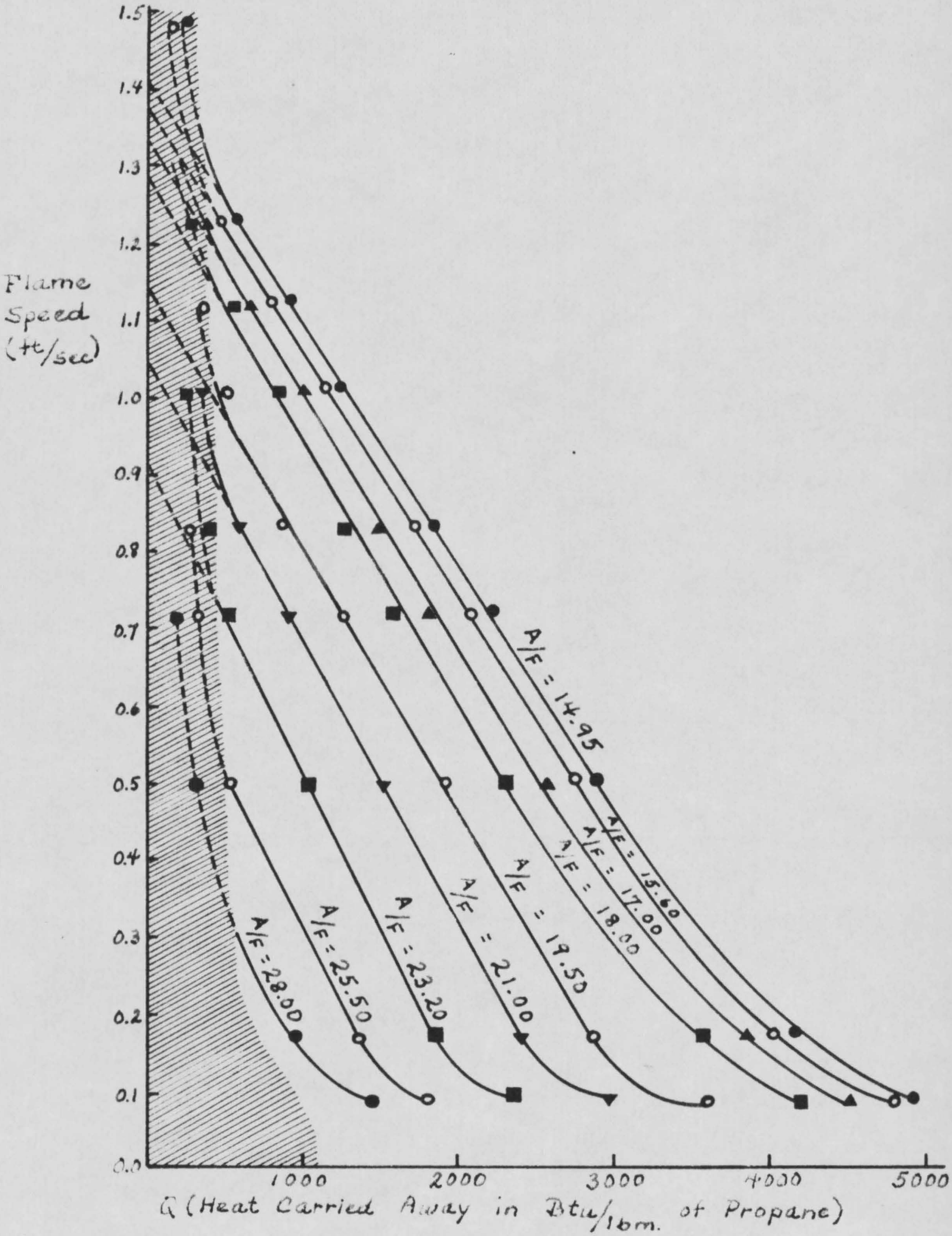

Figure 3.19 Flame Speed as a Function of Q for Different A/F Ratios on the Lean Side of A/F = 14.95

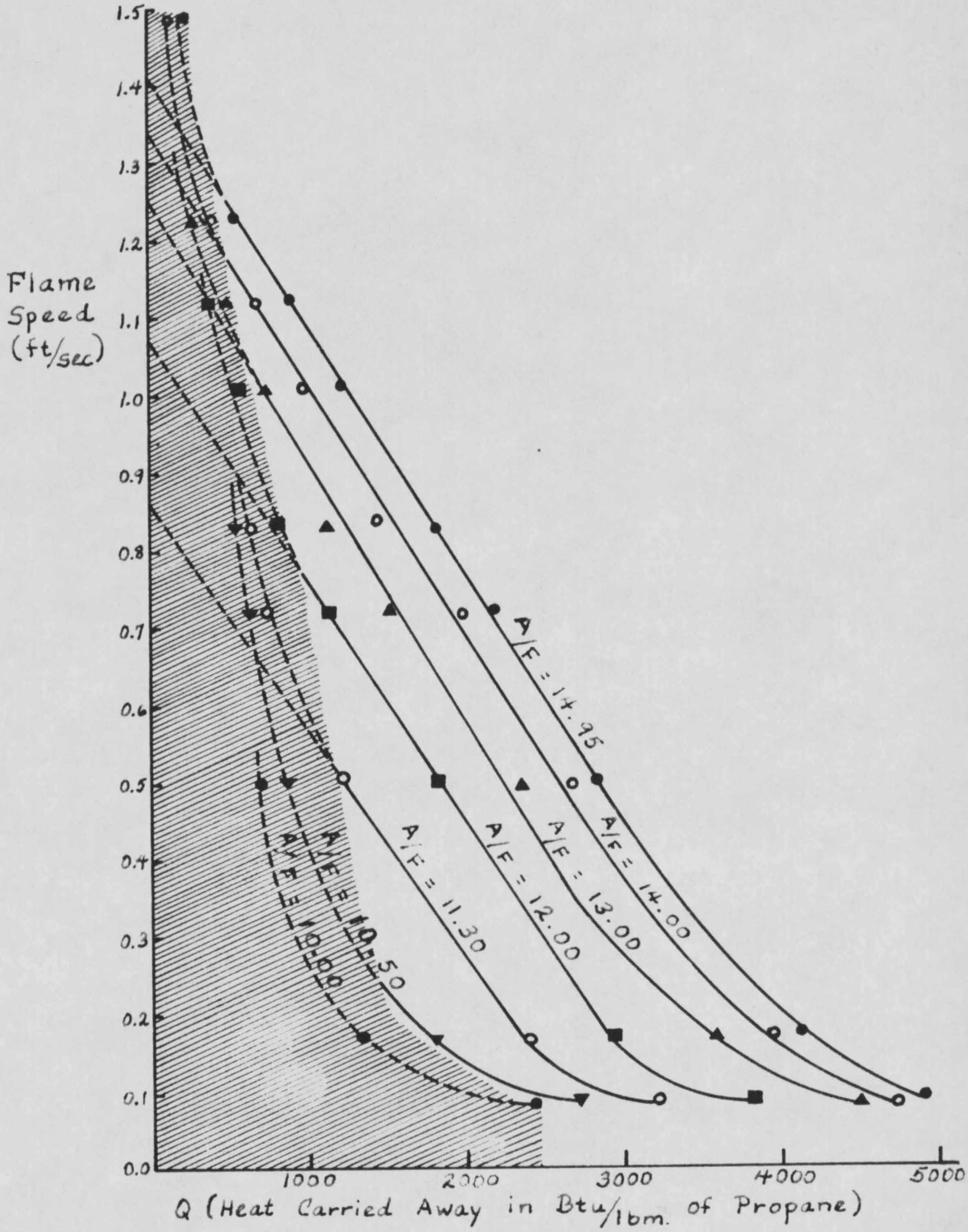

Figure 3.20 Flame Speed as a Function of Q for Different A/F Ratios on the Rich Side of A/F = 14.95

It should also be noted that the individual cells in the cases where the mixture speed is large differ from those in cases where it is small in that the cells are deeper as can be seen in Figure 3.12. This can be explained by the fact that the flame speed is the component of the mixture velocity normal to the flame front, and that this component is the same for a given air/fuel ratio, regardless of the mixture speed.

CHAPTER IV

CONCLUSIONS AND RECOMMENDATIONS

The two-inch diameter porous disc burner is a highly flexible system for both studying laminar flame speeds over a fairly extended range for which flat flames are obtainable and for studying laminar flame front stability. The two most significant features which contributed to the excellent performance of this burner were: first, the establishment of an adequate pressure drop across the porous discs by selection of the proper filtering porosity and filter thickness and second, the attainment of uniform cooling in the discs through the use of a series of concentric water-cooling jackets.

The use of the water-cooling system in conjunction with establishing the limiting case of zero temperature gradient is very important since incongruities in the flame structure appeared when the temperature gradient was not zero.

The method used for sizing magnesium oxide dust particles by first passing the dust-laden air/fuel mixture through a 15 micron filter greatly assisted in eliminating particles larger than 15 microns prior to allowing the mixture to enter the burner housing and is felt to be highly satisfactory. However, inasmuch as the particle track photography was unable to detect the magnesium oxide dust, it is believed that a more powerful light source should be used. In this case, the particles emanating from the burner port were measured with the aid of a microscope after being collected on an oiled glass slide. The particles were found to be as large as but no larger than eight microns in diameter, thereby substantiating the fact that the available particle track equipment as it exists at present is unable to photograph particles of this size or smaller.

It is believed that the flat flame burner developed for this thesis project represents a satisfactory system for use in the study of laminar flame propagation. The system is highly suited for the study of combustion at air/fuel ratios ranging from 7 to 30.

One possible improvement should be noted. G. Dixon-Lewis and G. L. Isles (15-17) suggest a way of reducing the likelihood of the flame being quenched by the cool areas around it through the use of an externally heated gauze or perforated plate above the burner housing.

It is strongly recommended that a corrugated flat flame burner (modeled after Dr. Powling's) designed to include installation of thermocouples be constructed. The result would be an apparatus readily adaptable to particle track studies. The corrugated burner will pass particles as large as 180 microns. It is felt that the existing particle track apparatus is capable of detecting and recording the tracks of these larger particles.

A complete analysis of cellular flame phenomena is of interest. During the course of experimentation, definite observations were made which led to the conclusion that the size and number of the cells were dependent upon the air/fuel ratio and the mixture speed, V_u. The mixture speed becomes important in the case of the porous disc burner because different amounts of heat are automatically removed by the burner for different mixture speeds at the same air/fuel ratio. The formation of these cells is defined by the nodes between the cells. The number of cells increases as the air/fuel mixtures become leaner until corrugation of the flame front occurs, followed by complete smoothing out to produce a flat flame. Lewis and Von Elbe (18) suggest that preferential diffusion is the mechanism for this phenomenon. However, Botha and Spalding (1) questioned this possibility since cells are observed with mixtures of all compositions.

Markstein (19) states that cellular structure in turbulence-free approach streams may be interpreted as flame front instability. Markstein showed that irregularities in the flame front tend to become magnified by deviations of the stream lines from the parallel. Furthermore, the supposition is made that the inherent tendency to instability is countered in some cases by an effect on the local flame speed of the resulting flame front curvature. Thus the divergence of the stream lines explains how it is possible for a flame cell to be stabilized in a stream where the mean velocity is greater than the maximum flame speed. It is concluded here that a complete explanation of cellular phenomena must be, at least in part, concerned with aerodynamic parameters.

As was noted in this thesis, the formation of concentric cellular rings and their subsequent rotation could be investigated by studying the effects of externally imposed disturbances.

Another point which is worthy of further study is the strikingly stable appearance of the cells on the lean side of stoichiometric (region IV of Figure 3.17) as was noted on page 47.

Finally, it should be mentioned that the porous disc burner offers an accurate method of stabilizing flames on a one-dimensional basis for temperature profile studies (3-6), optical studies (14, 20, 24), and other related experiments in the field of combustion (10, 11).

SYMBOLS

A = area

A/F = air/fuel ratio by weight

B = constant

I F = indicated flow rate in volume per unit time

m = mass

$\dot{m}$ = mass flow rate

M = molecular weight

P = pressure

P_m = pressure at the meter

P_s = pressure at standard conditions

P_u = pressure in unburned region

Q = heat transferred in Btu/lbm of propane

R = specific gas constant = R_o/M

R_o = universal gas constant

S_u = laminar adiabatic flame speed

T = temperature

T_b = temperature in the burned region

T_f = final temperature

T_o = initial temperature

T_u = temperature in the unburned region

t = time

V = total flow velocity

V_m = velocity at the meter

V_s = velocity at standard conditions

V_u = velocity in the unburned region

ρ = density

ρ_m = density at the meter

ρ_o = initial density

ρ_s = density at standard conditions

REFERENCES

1. Botha, J. P. and D. Spalding, "The Laminar Flame Speed of Propane/Air Mixtures with Heat Extraction from the Flame," Proc. Roy. Soc. A, V. 225, 1954, p. 71.

2. Egerton, Sir Alfred and S. K. Thabet, "Flame Propagation: The Measurement of Burning Velocities of Slow Flames and the Determination of Limits of Combustion," Proc. Roy. Soc. A, V. 211, 1952, p. 445.

3. Friedman, R., "Measurement of the Temperature Profile in a Laminar Flame," Fourth Symposium on Combustion, William Wilkins and Co., Baltimore, Md., 1953, pp. 259-63.

4. Friedman, R. and A. Macek, "Combustion Studies of a Single Aluminum Particle," Ninth Symposium on Combustion, Academic Press, Inc., New York, 1963, p. 703.

5. Friedman, R. and J. Cyphers, "Flame Structure Studies III - Gas Sampling in a Low-Pressure Propane Air Flame," J. Chem. Phys., V. 23, 1955, p. 1875.

6. Fristrom, R. M., R. Prescott, and C. Grunfelder, "Flame Zone Studies III - Technique for the Determination of Composition Profiles of Flame Fronts," Comb. and Flame I, Butterworths, London, 1957, pp. 102-113.

7. Fristrom, R. M. and A. A. Westenberg, Flame Structure and Interpretation (To be Published).

8. Fristrom, R. M., R. Prescott, R. K. Neuman, and W. H. Avery, "Temperature Profiles in Propane - Air Flame Fronts," Fourth Symposium on Combustion, 1953, pp. 267-274.

9. Fristrom, R. M., W. H. Avery, R. Prescott, and A. Mattuck, "Flame Zone Studies by the Particle Track Technique I - Apparatus and Techniques," J. Chem. Phys., V. 22, 1954, pp. 106-109.

10. Fristrom, R. M., Comments and Bibliography on the Measurement of Burning Velocity, The Johns Hopkins University Applied Physics Laboratory, TG 481, 1963.

11. Hirschfelder, J. O., C. F. Curtiss, and R. B. Bird, Molecular Theory of Gases and Liquids, Chapter I, John Wiley and Sons, New York, 1954.

12. Hoelscher, H., "Studies in a New-Type of Flat Flame Burner," Jet Prop., V. 27, 1957, p. 1257.

13. Kaser, R. V., "An Experimental Investigation of the Stability of a Laminar 'Vee' Flame," Ph.D. Dissertation, University of Arizona, Tucson, Arizona, 1965.

14. Levy, A. and F. J. Weinberg, "Optical Flame Structure Studies: Some Conclusions Concerning the Propagation of Flat Flames," Seventh Symposium on Combustion, Butterworths, London, 1959, p. 296.

15. Dixon-Lewis, G. and G. L. Isles, "Flames in Mixtures of Methane and Air Near the Lower Limit of Inflammability," Transactions of the Faraday Society, V. 410, 1957, p. 193.

16. Dixon-Lewis, G. and G. L. Isles, "Limits of Inflammability," Seventh Symposium (International) on Combustion, Butterworths Scientific Publications, London, 1958, p. 475.

17. Dixon-Lewis, G. and G. L. Isles, "Flame Structure Studies: The Temperature Profile in a Flame Supported by a Hydrogen-Nitrogen-Oxygen Mixture, Determined with the Use of Both Thermocouple and Optical Methods," Eighth Symposium (International) on Combustion, Williams and Wilkins Company, Baltimore, Md., 1962, p. 448.

18. Lewis, B. and G. Von Elbe, Combustion, Flames, and Explosion of Gases, Academic Press, New York, 1961.

19. Markstein, G. H., "Experimental and Theoretical Studies of Flame-Front Stability," Journal of the Aeronautical Sciences, V. 18, 1951, p. 199.

20. Pandya, T. P. and F. Weinberg, "The Study of the Structure of Laminar Diffusion Flames by Optical Methods," Ninth Symposium (International) on Combustion, Academic Press, New York, 1963, pp. 587-596.

21. Powling, J., "A New Burner Method for the Determination of Low Burning Velocities and Limits of Inflammability," Fuel, V. 28, 1949, p. 25.

22. Pyle, Edmund B., III, "Investigation and Modification of Secondary Air Flow on the University of Arizona Combustion Tunnel," M.S. Thesis, University of Arizona, Tucson, Arizona, 1964.

23. Smith, F., "Problems of Stationary Flames," Chem. Rev., 1930, p. 389.

24. Weinberg, F. J., "Application of Optical Methods to Combustion Research," Sixth Symposium (International) on Combustion, Reinhold Company, New York, 1956, p. 765.

25. Wright, F., "The Particle Track Method of Tracing Fluid Streamlines," The Jet Propulsion Laboratory, Cal. Tech. Progress Report, 3-23, 1951.